Electrophoresis

WILEY-VCH

ELECTROPHORESIS

RESEARCH ARTICLE

Electrophoresis of Charged Dielectric Droplet With Ion Concentration Polarization Effect

Yunfan Huang | Moran Wang

Department of Engineering Mechanics and SKL of APS, Tsinghua University, Beijing, China

Correspondence: Moran Wang (mrwang@tsinghua.edu.cn)

Received: 23 February 2026 | **Revised:** 30 April 2026 | **Accepted:** 28 May 2026

ABSTRACT

Droplet electrophoresis is one of the most commonly used methods for measuring the charge at two-liquid interfaces. However, there is still a lack of analytical solutions that consider the ion concentration polarization mechanism with asymmetric ion distribution under high surface charge. Based on the thin electric double layer assumption, we construct the asymptotic form of the macroscopic model of dielectric droplet electrophoresis and establish the coarse-grained effective interface condition across the diffuse layer regions through the heuristic treatment extending the method of matched asymptotic expansion, revealing the coupling mechanism between ion concentration polarization and permittivity-induced inhomogeneous charging. An analytical solution under the weak-external-field limit is provided, demonstrating a nonmonotonic dependence of electrophoretic mobility on the ζ potential under weak external electric fields. By integrating previous experimental results on droplet electrophoresis, a concise and physically meaningful quantitative model of the charging mechanism for general nonpolar oil is established.

1 | Introduction

Droplet electrophoresis is one of the most popular approach to measure the liquid–liquid interface charge, while the theoretical interpretation of its electrophoretic mobility still shows limitations [1, 2], in respect of physical and methodological aspects.

On the one hand, most of previous experimental works make the assumption of the so-called *droplet solidification*, which refers to the similar behaviors of droplet electrophoresis to the solid particle electrophoresis and is usually attributed to the surface-active impurities [3]. However, the modern experimental technique in preparing and processing the droplet emulsions is able to avoid the interference of surface-active impurities [4], while the ion transport within electrical double layer may also give rise to the similar "solidification"-like phenomena due to the ion concentration polarization phenomena [3, 5–7]. Therefore, the effect of interfacial ion transport around the mobile interface on droplet electrophoretic mobility should be carefully considered.

Compared to other systems such as metallic droplet and gas bubble, the dielectric droplet may show quite different electrophoretic mobility scalings. On the one hand, the induced charge effect at interface is much weaker than the metallic cases due to the finite (and essentially zero) conductivity ratio $\mathcal{K}_r \equiv \mathcal{K}_{\text{int}}/\mathcal{K}_{\text{ext}} \equiv \bar{\mathcal{K}}/\mathcal{K}$ and relatively low permittivity ratio [8, 9]. On the other hand, it has finite permittivity ratio $\varepsilon_r \equiv \varepsilon_{\text{int}}/\varepsilon_{\text{ext}} \equiv \bar{\varepsilon}/\varepsilon$ and dynamic viscosity ratio $\eta_r \equiv \eta_{\text{int}}/\eta_{\text{ext}} \equiv \bar{\eta}/\eta$, where the weak but finite induced charge effect may couple with the ion polarization effect and show a continuous scaling transition when the finite viscosity ratio is considered [8, 10]. It is worth noting that the ion concentration polarization effect denoted here is treated in another form called *convective conduction* in early works [8], which, however, also take advantages of the Helmholtz double layer model to reduce the theoretical complexity. This simplification qualitatively captures the essential underlying physics of *surface conduction*, but ignores the inhomogeneous charge distribution along radius direction when the induced charge effect is taken into consideration, which may impact the mobility scaling in the low ζ limit.

On the other hand, the present quantitative studies that incorporate the aforementioned ion transport around the finite-viscosity droplet interfaces usually rely on the numerical solutions based on the weak field linearization, which is not convenient enough for practical use in electrophoresis experiments and may not be able to provide the analytical insights into the underlying physics [6, 11, 12]. Generally speaking, the difficulties in theoretical treatment of droplet electrophoresis usually lie in the cases of high interfacial charging $\zeta/V_T \gg 1$, strong external field $\mathcal{B}_E \gtrsim 1$, or thick double layer $\lambda_D/a \equiv 1/\kappa a \gtrsim 1$ where the nonlinear transport phenomena within the electrical double layer are expected to be significant [13–15]. Here, ζ is the zeta potential of charged interface, $V_T \equiv k_B T/e$ is called the thermal voltage (~ 25 mV under room temperature), $\mathcal{B}_E \equiv E_\infty a/V_T$ is the dimensionless external electric field, while λ_D and a are the Debye length and droplet radius ($\sim 1-100\,\mu$m), respectively.

The perturbation method is often used to obtain the analytical solution or at least the simplified problem set under certain parameter limit. According to the different choices on the perturbation parameters, the perturbation methods for colloidal particle electrophoresis can be classified into three categories, that is, Henry–Overbeek–Booth method in the low ζ potential limit [16–20], O'Brien–White method in the low $\mathcal{B}_E$ limit for solid particles [21, 22] or liquid droplets [5, 6, 11, 23–25], and Frumkin–Levich–Dukhin method in the thin double layer limit [8–10, 26–31]. Though sharing the same object of linearization, those three methods show quite large differences in both leading-order formulation and theoretical applicability.

For dielectric droplets under weak fields, which is most commonly met in droplet electrophoresis measurements, the analytical solution that is able to incorporate the ion concentration polarization effect is still lacking, especially in those studies based on the Henry–Overbeek–Booth and O'Brien–White approaches. Here, we mentioned several examples to address the relevant progress in recent years. Mahapatra and Hill adopted Debye–Hückel approximation to the low-surface charge case (i.e., low ζ potential limit) which considers the moving ion at surface and generaizes Booth's theory to arbitrary Damköhler number [32]. Majhi et al. adopted the numerical methods to solve the perturbated governing equations under the assumption of weak field (i.e., the low $\mathcal{B}_E$ limit) which incorporates the correlation effects induced by the finite-size surfactant ion [33], while Hill utilized the similar method to study the effect of interfacial-exchange kinetics, interfacial-charge mobility, and Marangoni effects [34] following Baygents and Saville [6]. Ohshima further adopted both assumptions to investigate ion adsorption and Marangoni effects [35]. For those analytical solutions, the assumptions of low interface ζ potential and linear proposition of external fields and initial double layer fields are used, which typically ignored the *ion concentration polarization* effect [36]. In particular, the analytical solution of dielectric droplet electrophoresis that can be extended to the relatively highly charged interfaces is still lacking, where the ion concentration polarization effect may play a significant role. This not only limits the applicability of those analytical solutions in droplet electrophoresis measurements, but also gives rise to the discontinuity of the mobility scaling at low ζ and even unreasonable predictions in the low droplet viscosity limit [19, 37, 38].

Since the thin double layer limit can be usually satisfied in the droplet electrophoresis measurement [4, 39, 40], the Frumkin–Levich–Dukhin method, which gives the leading-order theory of a coarse-grained model with effective interface conditions encapsulating the complex nonlinear transport within the double layer and is able to indicate the physical mechanism at the double layer scale, is more suitable for the analytical solution of highly charged droplet electrophoresis with ion concentration polarization effect. Since 1990s, there have been a series of works on the Frumkin–Levich–Dukhin method for the droplet electrokinetics (EK) or electrohydrodynamics (EHD), including conducting droplets with either adsorption-induced interface charging under strong fields $\mathcal{B}_E \gtrsim 1$ [30, 41], conducting droplets with partition-induced interface charging under weak fields $\mathcal{B}_E \ll 1$[31, 42], vesicles between two conducting fluids with finite interphase permeability [42], and metallic droplets with induced charge effects [9, 43]. In particular, Schnitzer and Yariv first derive the classical Taylor–Melcher EHD model as the large-field and thin double layer limit of the EK equations through the method of matched asymptotic expansion. This serves as a milestone that resolve the several issues on Debye diffuse layer and screening-induced electroneutrality related to the ubiquitous "leaky dielectric" approximation [44].

In this work, we aim to provide the analytical solution of electrophoresis of highly charged dielectric droplet with ion concentration polarization effect following the Frumkin–Levich–Dukhin method. Our work gives the solution that is beyond the low ζ potential limit that is often utilized in previous studies, and provides the analytical insights into the coupling mechanism between ion concentration polarization and permittivity-induced inhomogeneous charging at the moderate $\mathcal{B}_E$ regime. It is noteworthy that this paper combines several assumptions listed as follows to deduce the final asymptotic equations: spherical undeformed droplet, thermodynamically polarizable interface, symmetric electrolyte with equal ion diffusivities ($D_+^* = D_-^* = D^*$) and fully interface-mobile feature, thin EDL ($\lambda_D/a \ll 1$), physically induced charge perturbation with instantaneous chemical equilibrium, and moderate external field ($\delta\mathcal{B}_E \ll \zeta_0$), while the explicit analytical solutions are further given under the weak-field/low-zeta-potential limits.

The paper is organized as follows. In particular, we closely follow the method utilized in the bubble electrophoresis analysis in previous work [10]. In Section 2, we present the governing equations and the coarse-grained model for the dielectric droplet electrophoresis. In Section 3, we introduce the perturbation method for the analytical solution of the droplet electrophoresis. In Section 4, we present the analytical solution of the droplet electrophoresis, discuss the scaling behaviors of the electrophoretic mobility, and shows its application to charging mechanism model for nonpolar oil as illustration. The conclusions are given in Section 5.

2 | Mathematical Models

In the following theoretical formulation, the dimensional forms denoted by X^* will be used, with the corresponding dimensionless forms denoted by X.

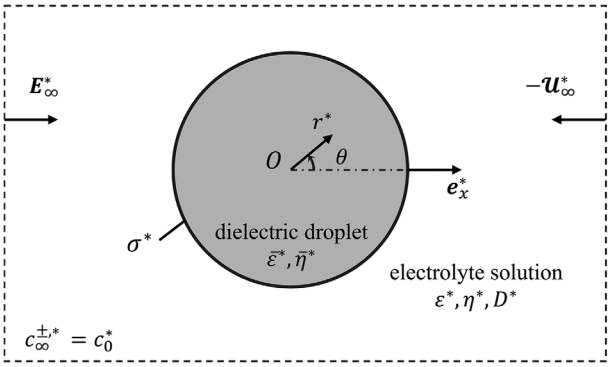

FIGURE 1 | System schematics of dielectric droplet electrophoresis.

2.1 | Physical Problems and Descriptions

As shown in Figure 1, considering a dielectric droplet in electrolyte solution, whose radius is R^* and the surface charge density is maintained at a constant value σ^*, the electrophoretic velocity under the external electric field E^*_∞ is denoted by U^*. The permittivity and dynamic viscosity of electrolyte solution (called *exterior*) are denoted by ε^* and η^*, while those properties of dielectric droplet (called *interior*) are denoted by $\bar{\varepsilon}^*$ and $\bar{\eta}^*$. For simplicity, the electrolyte is chosen as z^*:z^* type with net charge of $\pm z^* e^*$, the concentration is c^*_0, and the molecular diffusivities of the cation and the anion are assumed the same, indicated by D^*.

For the exterior region with the electrolyte solution, the continuity equation and low-*Re* Stokes equation for steady incompressible flows are written as

$$\nabla^* \cdot \boldsymbol{u}^* = 0, \tag{1}$$

$$\nabla^* p^* = \eta^* \nabla^{*2} \boldsymbol{u}^* - \rho^*_e \nabla^* \varphi^*. \tag{2}$$

Here, $\rho^*_e = z^* F^* (c^{+*} - c^{-*})$ is the volume charge density, and $F^* = e^* N^*_A$ is the Faradaic constant. The electric potential φ^* satisfied electrostatic Poisson equation

$$-\varepsilon^* \nabla^{*2} \varphi^* = \rho^*_e. \tag{3}$$

Therefore, the Stokes equation can be also written as

$$\nabla^* \cdot \left(-p^* \boldsymbol{I}^* + \boldsymbol{T}^{\eta^*} + \boldsymbol{T}^{e^*}\right) = 0, \tag{4}$$

where $\boldsymbol{T}^{\eta^*}$ and $\boldsymbol{T}^{e^*}$ are the Newtonian shear stress and Maxwell stress tensors, respectively,

$$\boldsymbol{T}^{\eta^*} = \eta^* \left[\nabla^* \boldsymbol{u}^* + (\nabla^* \boldsymbol{u}^*)^T\right], \tag{5}$$

$$\boldsymbol{T}^{e^*} = \varepsilon^* \left[\boldsymbol{E}^* \boldsymbol{E}^* - \frac{1}{2}(\boldsymbol{E}^* \cdot \boldsymbol{E}^*) \boldsymbol{I}^*\right]. \tag{6}$$

Here, the electric field $\boldsymbol{E}^* = -\nabla^* \varphi^*$ is used. Ion concentration fields $c^{\pm *}$ related to the charge density satisfy the Nernst–Planck equations

$$\nabla^* \cdot \boldsymbol{j}^{*\,*}_\pm = 0, \tag{7}$$

where $\boldsymbol{j}^{*\,*}_\pm = -D^* \nabla^* c^{\pm *} \mp z^* F^* c^{\pm *} \nabla^* \varphi^* + \boldsymbol{u}^* c^{\pm *}$ are the concentration flux of cations and anions.

For the interior region with dielectric droplet, the continuity equation and momentum equation are similarly written as

$$\nabla^* \cdot \bar{\boldsymbol{u}}^* = 0, \tag{8}$$

$$\nabla^* \bar{p}^* = \eta^* \nabla^{*2} \bar{\boldsymbol{u}}^*. \tag{9}$$

Here, the ion concentration and charge density are both zero, while the electric potential satisfies the Laplace equation

$$\nabla^{*2} \bar{\varphi}^* = 0. \tag{10}$$

Taking a referenced frame that is moving with the electrophoretic droplet, we establish a spherical coordinate (r^*, θ, υ) with the center $r^* = 0$ in coincidence with the droplet center and the direction of $\boldsymbol{e}^*_r$ at $\theta = 0$ as well as the x-axis pointing to the direction of the external electric field $\boldsymbol{E}^*_\infty$. From the symmetry analysis of the system setup, the physical fields are independent of υ, in which the velocity field is denoted by $\boldsymbol{u}^* \equiv u^* \boldsymbol{e}^*_r + \upsilon^* \boldsymbol{e}^*_\theta$. To write down the boundary conditions at infinity and the interface conditions at the droplet interface, the following assumptions are taken:

(i) The interface tension is uniform and high enough to main the spherical shape of the droplet, then $r^* = R^*$ corresponds to the droplet surface.

(ii) The interface is thermodynamically polarizable, that is, the interphase ion flux is zero under steady conditions.

(iii) The surface charge density is uniform and fixed at σ^* during the electrophoretic motion.

Then, the boundary conditions at infinity $r^* \to \infty$ are written as

$$\boldsymbol{u}^* \to -U^* \boldsymbol{e}^*_x, \tag{11}$$

$$-\nabla^* \varphi^* \to E^*_\infty \boldsymbol{e}^*_x, \tag{12}$$

$$c^{\pm *} \to c^*_0. \tag{13}$$

And the interface conditions at the droplet surface $r^* = R^*$ are

$$u^* = \bar{u}^* = 0, \tag{14}$$

$$\upsilon^* = \bar{\upsilon}^*, \tag{15}$$

$$\eta^* \left(\frac{\partial \upsilon^*}{\partial r^*} - \frac{\upsilon^*}{R^*}\right) - \bar{\eta}^* \left(\frac{\partial \bar{\upsilon}^*}{\partial r^*} - \frac{\bar{\upsilon}^*}{R^*}\right) = \sigma^* \frac{1}{R^*} \frac{\partial \varphi^*}{\partial \theta}, \tag{16}$$

$$\varepsilon^* \frac{\partial \varphi^*}{\partial r^*} - \bar{\varepsilon}^* \frac{\partial \bar{\varphi}^*}{\partial r^*} = -\sigma^*, \tag{17}$$

$$\boldsymbol{e}^*_r \cdot \boldsymbol{j}^{*\,*}_\pm = 0. \tag{18}$$

The above equations are, in order, the conditions for interface impenetrability, tangential velocity continuity, balance of tangential stress, matching of normal electric displacement, and thermodynamic polarizability. To enclose the above problem, the force balance condition of droplet should be satisfied

$$\oiint_{r^*=R^*} \left(-p^*\boldsymbol{I}^* + \boldsymbol{T}^{\eta^*} + \boldsymbol{T}^{e^*}\right)\cdot \boldsymbol{e}_r^* dA^* = 0. \tag{19}$$

Noting that $\nabla^*\cdot\left(-p^*\boldsymbol{I}^* + \boldsymbol{T}^{\eta^*} + \boldsymbol{T}^{e^*}\right) = 0$, the integral surface can be chosen as the arbitrary one that encloses the droplet. To this end, once the external field E_∞^* and material properties are prescribed, the electrophoretic velocity $\mathcal{U}^*$ of the dielectric droplet is obtained by solving the above problem, then giving the electrophoretic mobility $\mathcal{U}^*/E_\infty^*$.

2.2 | Dimensionless Formulation

To give the dimensionless form, here we choose the droplet radius R^*, bulk concentration of electrolyte solution c_0^*, thermal voltage $\varphi^* \equiv V_T^* = k_B^* T^*/z^* e^*$ as the characteristic length, concentration, and electric potential. The corresponding Maxwell stress $T^{e^*} = \varepsilon^*\varphi^{*2}/R^{*2}$ is used as the characteristic stress, and the velocity corresponding to the stress $u^* = R^* T^{e^*}/\eta^* \equiv \varepsilon^*\varphi^{*2}/(\eta^* R^*)$ is recognized as the characteristic velocity. In this case, the droplet surface corresponds to $r = r^*/R^* \equiv 1$, the dimensionless external electric field is $\mathcal{B} \equiv \mathcal{B}_E = E_\infty^* R^*/\varphi^*$, the electrophoretic velocity is $\mathcal{U} = \mathcal{U}^*/u^*$, and the surface charge density is $\sigma = \sigma^*/(\varepsilon^*\kappa^*\varphi^*)$. Here, κ^* is the reciprocal of Debye length $\lambda_D^* \equiv \kappa^{*-1}$, satisfying

$$\kappa^{*2} = \frac{2z^* e^* c_0^*}{\varepsilon^*\varphi^*}. \tag{20}$$

The dimensionless form of the above problem is then given as follows.

For the exterior region, the continuity equation and Stokes equation of steady incompressible flow can be written as

$$\nabla\cdot\boldsymbol{u} = 0, \tag{21}$$

$$\nabla p = \nabla^2\boldsymbol{u} + \nabla^2\varphi\nabla\varphi. \tag{22}$$

The electrostatic Poisson equation is

$$-2\delta^2\nabla^2\varphi = c^+ - c^-, \tag{23}$$

where $\delta = (\kappa^* R^*)^{-1}$. The steady Nernst–Planck equations are written as

$$\nabla\cdot\boldsymbol{j}^\pm + \mathcal{A}\boldsymbol{u}\cdot\nabla c^\pm = 0. \tag{24}$$

Here, $\boldsymbol{j}^\pm = -\nabla c^\pm \mp c^\pm\nabla\varphi$ are the sum of diffusive and electromigrative flux of cations and anions, and $\mathcal{A}$ is the hydrodynamic viscous coupling constant

$$\mathcal{A} = \frac{\varepsilon^*\varphi^{*2}}{\eta^* D^*} \sim \frac{\varepsilon^*\varphi^{*2} d^*}{k_B^* T^*} \lesssim 0.5, \tag{25}$$

where d^* is the hydrodynamic diameter of typical solute ions [45]. For the interior region, the continuity equation, momentum equation, and electrostatic Laplace equation are written as

$$\nabla\cdot\bar{\boldsymbol{u}} = 0, \tag{26}$$

$$\nabla\bar{p} = \eta_r\nabla^2\bar{\boldsymbol{u}}, \tag{27}$$

$$\nabla^2\bar{\varphi} = 0. \tag{28}$$

The interface conditions at the droplet surface $r = 1$ are

$$u = \bar{u} = 0, \tag{29}$$

$$v = \bar{v}, \tag{30}$$

$$\left(\frac{\partial v}{\partial r} - v\right) - \eta_r\left(\frac{\partial \bar{v}}{\partial r} - \bar{v}\right) = \delta^{-1}\sigma\frac{\partial\varphi}{\partial\theta}, \tag{31}$$

$$\frac{\partial\varphi}{\partial r} - \varepsilon_r\frac{\partial\bar{\varphi}}{\partial r} = -\delta^{-1}\sigma, \tag{32}$$

$$\frac{\partial\varphi}{\partial\theta} = \frac{\partial\bar{\varphi}}{\partial\theta}, \tag{33}$$

$$\boldsymbol{e}_r\cdot\boldsymbol{j}^\pm = 0, \tag{34}$$

while the boundary conditions at infinity $r\to\infty$ are

$$\boldsymbol{u} \to -\mathcal{U}\boldsymbol{e}_x, \tag{35}$$

$$\nabla\varphi \to -\mathcal{B}\boldsymbol{e}_x, \tag{36}$$

$$c^\pm \to 1. \tag{37}$$

The force balance of the droplet is written as

$$\oiint_{r=1} (-p\boldsymbol{I} + \boldsymbol{T}^\eta + \boldsymbol{T}^e)\cdot\boldsymbol{e}_r dA = 0. \tag{38}$$

To illustrate the coupling relations between physical fields, the variable transformation from ionic concentrations $c^\pm$ to the apparent salt concentration $c = (c^+ + c^-)/2$ and apparent charge density $q = (c^+ - c^-)/2$ (i.e., the *c-q representation*) is conducted, and the concentration fluxes are transformed into the concentration flux $\boldsymbol{j} = (\boldsymbol{j}^+ + \boldsymbol{j}^-)/2$ and electric current density $\boldsymbol{i} = (\boldsymbol{j}^+ - \boldsymbol{j}^-)/2$ correspondingly. Then, the fluxes are written as

$$\boldsymbol{j} = -\nabla c - q\nabla\varphi, \quad \boldsymbol{i} = -\nabla q - c\nabla\varphi. \tag{39}$$

The corresponding conservation equations for concentration c and charge q are as follows:

$$\nabla\cdot\boldsymbol{j} + \mathcal{A}\boldsymbol{u}\cdot\nabla c = 0, \quad \nabla\cdot\boldsymbol{i} + \mathcal{A}\boldsymbol{u}\cdot\nabla q = 0. \tag{40}$$

The electrostatic Poisson equation is then written in a more compact form

$$\delta^2\nabla\varphi = -q. \tag{41}$$

The interface conditions for c and q at $r = 1$ are

$$\boldsymbol{e}_r \cdot \boldsymbol{j} = 0, \quad \boldsymbol{e}_r \cdot \boldsymbol{i} = 0, \tag{42}$$

while the boundary conditions at $r \to \infty$ are

$$c \to 1, \quad q \to 0. \tag{43}$$

The complete equation set for the problem of dielectric droplet electrophoresis is obtained, whose difficulty in theoretical treatment lies in the nonlinear coupling transport terms in the conservation equations for c, q, and $\boldsymbol{u}$.

3 | Methods of Matched Asymptotic Expansion

This section will first outline the overall approach of matched asymptotic expansions. The form of the interfacial conditions and the physical fields to be determined will be then derived by solving the leading-order solution within the inner region of the electric double layer. Subsequently, higher-order solutions within the inner region of the electric double layer will be solved to close the effective interfacial conditions for stress matching across the outer regions, following by the effective boundary conditions for the normal flux of the higher-order concentration field. In particular, we will first ignore the induced charge effect, which is essentially following the Schnitzer's work except for a finite viscosity of droplet [10]. Once considering the externally induced charge due to the finite permittivity of droplet, a heuristic treatment incorporating higher-order terms into the leading-order analysis which extends the standard method of matched asymptotic expansion is given. It is shown that the inhomogeneous charging at the liquid–liquid interface will cause the tangential electric field to no longer be uniform in the direction normal to the double layer. This will result in the dielectric droplet exhibiting an ion concentration polarization effect under low surface potential conditions, which differs from that of bubbles [10]. In the following, we adopt the assumption of the thin double layer limit $\delta \equiv \lambda_D^*/R^* \ll 1$, and assume that the external electric field is not too strong (which we call the *moderate* strength), such that $\delta\mathcal{B} \ll \min\{1, \zeta_0\}$, where ζ_0 denotes the dimensionless zeta potential of the dielectric droplet surface in the absence of external field. Note that very strong fields $\mathcal{B} \gg 1$ would contribute a field-induced charge approaching the spontaneous interface charge, leading to the nonlinear convective effects.

3.1 | Region Decomposition and Matching Condition

For the electrophoresis of electric droplet, the thin double layer limit is usually satisfied. As a nonlinear transport problem with scale disparity at mobile interface, the method of matched asymptotic expansion (i.e., the aforementioned Frumkin–Levich–Dukhin method) is a more feasible approach to obtain the solution compared with direct numerical simulation. Besides, the resulting coarse-grained problem with effective interface conditions will uncover the coupling transport phenomena at the interface, and also presents a more simple form serving as the foundation for further upscaling numerical simulation. In general, this method takes the assumption of thin double layer, solves the physical fields within the diffuse layer (called *inner region*), and then matches the solution with the physical fields outside the diffuse layer (called *outer region*).

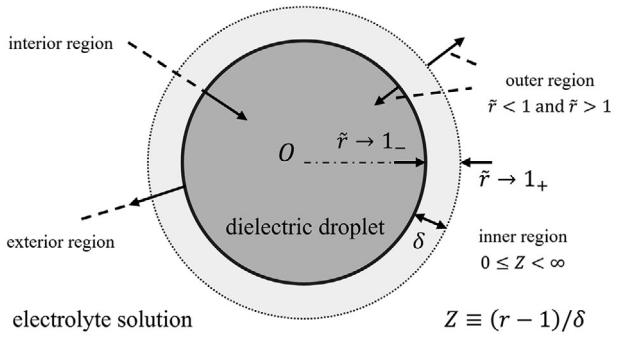

FIGURE 2 | Schematics of matched symptotic expansion for dielectric droplet electrophoresis.

Here, we assume the diffuse layer thickness is much less than the droplet radius R^*, that is, $\delta \ll 1$, and the other parameters are of order unity. As shown in Figure 2, following the typical treatment in previous studies [9, 10], for the exterior region $r > 1$, we set the inner variable $Z = (r-1)/\delta$ to describe the transport within the diffuse layer, and the outer variable $\tilde{r}$ to describe the transport behavior outside the diffuse layer. Here, $Z = 0$ corresponds to the liquid–liquid interface at $r = 1$, and $\tilde{r} \to 1_+$ corresponds to the outer edge of the diffuse layer at $Z \to \infty$, while $\tilde{r} \to 1_-$ corresponds to the inner edge of the diffuse layer at $Z = 0$. According to the previous definition, $r > 1$ and $0 < r < 1$ are referred to as the exterior and interior regions of the interface, respectively, and $0 \le Z < \infty$ is referred to as the inner region, while $\tilde{r} > 1$ and $0 < \tilde{r} < 1$ represent the outer regions.

As the foundation for the asymptotic expansion and order matching of the governing equations (especially the Stokes equations), the representation of the gradient operator, as well as the Laplacian of scalars and vectors in the local coordinate system with intrinsic variables as the independent variables, is first analyzed. Using the linear transformation between the inner and outer variables $r = 1 + \delta Z$, it is yielded that

$$\frac{\partial}{\partial r} = \frac{1}{\delta}\frac{\partial}{\partial Z}$$

and

$$\nabla^2 \doteq \frac{1}{\delta^2}\frac{\partial^2}{\partial Z^2} + \frac{2}{\delta}\frac{\partial}{\partial Z} - 2Z\frac{\partial}{\partial Z} + \frac{1}{\sin\theta}\frac{\partial}{\partial\theta}\left(\sin\theta\frac{\partial}{\partial\theta}\right) + \frac{1}{\sin^2\theta}\frac{\partial^2}{\partial v^2} + \mathcal{O}(\delta).$$

Considering the system symmetry around the x-axis, any physical field in the spherical coordinate system can be written as $\boldsymbol{A} \equiv A_r\boldsymbol{e}_r + A_\theta\boldsymbol{e}_\theta$, and then

$$(\nabla^2\boldsymbol{A}) \cdot \boldsymbol{e}_r = \nabla^2 A_r - 2A_r + \mathcal{O}(\delta),$$

$$(\nabla^2\boldsymbol{A}) \cdot \boldsymbol{e}_\theta = \nabla^2 A_\theta - \frac{A_\theta}{\sin^2\theta} + 2\frac{\partial A_r}{\partial\theta} + \mathcal{O}(\delta).$$

Here, the physical fields in the inner region have taken the limit of $r \to 1_+$, and $\mathcal{O}(\delta)$ is defined corresponding to the limit $\delta \to 0$. For

simplicity, later on we will use r to represent the outer variable $\tilde{r}$ in the outer region, and use Z when referring to the inner region.

For the inner region, from the electrostatic interface condition (32) and Poisson equation (23), the potential field φ and concentration field $c^{\pm}$ are both of order $\mathcal{O}(1)$. From the interface condition of shear stress (31) the tangential velocity v is of order $\mathcal{O}(1)$, and the normal velocity u can be further evaluated at $\mathcal{O}(\delta)$ from the continuity equation (21) and interface condition of velocity (29). From the normal component of Stokes equation (22) at the order of $\mathcal{O}(\delta^{-3})$, the pressure is evaluated at $\mathcal{O}(\delta^{-2})$. The physical fields within the diffuse layer region can be then expanded as follows:

$$\varphi = \Phi_0(Z,\theta) + \delta\Phi_1(Z,\theta) + \ldots,$$
$$c^{\pm} = C_0^{\pm}(Z,\theta) + \delta C_1^{\pm}(Z,\theta) + \ldots,$$
$$v = V_0(Z,\theta) + \delta V_1(Z,\theta) + \ldots,$$
$$u = \delta U_1(Z,\theta) + \ldots,$$
$$p = \delta^{-2}P_{-2}(Z,\theta) + \delta^{-1}P_{-1}(Z,\theta) + \ldots.$$

In the c–q representation, it is similarly written as

$$c = C_0(Z,\theta) + \delta C_1(Z,\theta) + \ldots,$$
$$q = Q_0(Z,\theta) + \delta Q_1(Z,\theta) + \ldots,$$
$$\boldsymbol{e}_r \cdot \boldsymbol{j} = J_0(Z,\theta) + \delta J_1(Z,\theta) + \ldots,$$
$$\boldsymbol{e}_r \cdot \boldsymbol{i} = I_0(Z,\theta) + \delta I_1(Z,\theta) + \ldots.$$

For any physical field f in the outer region $r > 1$, performing the expansion $f = f_0 + \delta f_1 + \ldots$, it is derived from the electrostatic Poisson equation (23) that

$$q_0 = 0, \quad q_1 = 0, \tag{44}$$

thus

$$c_0^{\pm} = c_0, \quad c_1^{\pm} = c_1. \tag{45}$$

Substituting into the fluxes of concentration and charge (39), it yields

$$\boldsymbol{j}_0 = -\nabla c_0, \quad \boldsymbol{i}_0 = -c_0\nabla\varphi_0. \tag{46}$$

From the conservation equation of concentration and charge (40), it is indicated that c_0 and φ_0 obey the advection–diffusion equation and charge conservation equation, respectively,

$$\nabla^2 c_0 = \mathcal{A}\boldsymbol{u}_0 \cdot \nabla c_0, \tag{47}$$

$$\nabla \cdot (c_0\nabla\varphi_0) = 0. \tag{48}$$

And from the continuity equation (21) and Stokes equation (22), it is obtained that

$$\nabla \cdot \boldsymbol{u}_0 = 0, \tag{49}$$

$$\nabla p_0 = \nabla^2\boldsymbol{u}_0 + \nabla^2\varphi_0\nabla\varphi_0. \tag{50}$$

For the physical fields in the interior region $0 < r < 1$, it is similarly derived that

$$\nabla \cdot \bar{\boldsymbol{u}}_0 = 0, \tag{51}$$

$$\nabla\bar{p}_0 = \nabla^2\bar{\boldsymbol{u}}_0, \tag{52}$$

$$\nabla^2\bar{\varphi}_0 = 0. \tag{53}$$

The matching conditions between inner and outer solutions connect the physical fields within the diffuse layer in the limit of $Z \to \infty$ and those in the outer region in the limit of $r \to 1_+$ [46]. For the leading-order solutions, it is required that when $Z \to \infty$,

$$C_0^{\pm} \to c_0, \quad \Phi_0 \to \varphi_0, \quad V_0 \to v_0, \tag{54}$$

and the interface conditions of electrostatics (31) and shear stress (32) at $r = 1$ give

$$\frac{\partial\Phi_0}{\partial Z} \to 0, \quad \frac{\partial V_0}{\partial Z} \to 0. \tag{55}$$

For the higher-order solutions, it is required that when $Z \to \infty$,

$$\Phi_1 \to \varphi_1, \quad \frac{\partial\Phi_1}{\partial Z} \to \frac{\partial\varphi_0}{\partial r}, \quad C_1^{\pm} \to c_1, \quad \frac{\partial V_1}{\partial Z} \to \frac{\partial v_0}{\partial r}. \tag{56}$$

We will start with the outer region $r > 1$. From the $\mathcal{O}(\delta^{-1})$ terms of conservation equations of concentration and charge (40) it is given that at $r = 1$,

$$\frac{\partial c_0}{\partial r} = 0, \quad \frac{\partial\varphi_0}{\partial r} = 0. \tag{57}$$

Combining with the zeroth-order term of the advection–diffusion equation of concentration (47) and the corresponding boundary condition at infinity, it yields

$$c_0 \equiv 1. \tag{58}$$

Substituting into the zeroth-order term of charge conservation equation (48), the Laplace equation is derived

$$\nabla^2\varphi_0 = 0. \tag{59}$$

Taking the interface condition at $r = 1$ and boundary condition at infinity into consideration, it is obtained that

$$\varphi_0 = -\mathcal{B}\left(r + \frac{1}{2r^2}\right)\cos\theta, \quad q_0 = 0. \tag{60}$$

Therefore, the Stokes equation (50) is reduced to

$$\nabla p_0 = \nabla^2\boldsymbol{u}_0, \tag{61}$$

while the force balance constraint of droplet gives

$$\oiint_{r=1}\left(-p_0\boldsymbol{I} + \boldsymbol{T}_0^{\eta}\right)\cdot\boldsymbol{e}_r dA = 0. \tag{62}$$

Due to the triviality of the zeroth-order solutions for ion concentration and charge density fields in the outer region, the aforementioned ion concentration polarization behavior will couple with the velocity field and higher-order ion concentration fields. Besides, as we will see in the following subsections, the droplet electrophoresis is driven by a dual mechanism of effective

slip velocity and effective interfacial shear stress, replacing the single driving mechanism of effective slip velocity in the case of solid particle.

3.2 | Effective Interfacial Conditions: Ignoring Induced Charge Effect

The following will present the leading-order solution for the inner region of the electric double layer when the induced charge effect is ignored (as a higher-order effect). In particular, our formulation allows for a nonzero $\partial\Psi/\partial\theta$, therefore presenting a (slightly) more general formulation compared with previous work [10], which is essential for the induced charge effect to be considered in the next subsection. Here, σ is assumed to be a constant, which is the initial surface charge density contributed by the adsorbed solute ions at interface induced by the interfacial chemical reaction.

For the salt concentration and charge density distribution in the inner region, considering the $\mathcal{O}(\delta^{-1})$ terms in the conservation equation of concentration (24) is zero and noticing the interface condition at $Z = 0$ (34), the zeroth-order normal ionic flux J_0 is zero and the diffuse layer in the normal direction is in the electrochemical equilibrium [36]. Therefore, the leading-order solution of salt concentration obeys the Boltzmann distribution, whose specific form can be obtained once noticing the matching condition at $Z \to \infty$ (54)

$$C_0^{\pm} = c_0 \mathrm{e}^{\pm\Psi}, \tag{63}$$

here $\Psi \equiv \Phi_0 - \varphi_0$ which satisfies $\Psi \to 0$ when $Z \to \infty$. From the $\mathcal{O}(1)$ terms in the electrostatic Poisson equation (23), it is derived that

$$\frac{\partial^2\Psi}{\partial Z^2} = c_0 \sinh\Psi \Rightarrow \frac{\partial\Psi}{\partial z} = -2\sqrt{c_0}\sinh\frac{\Psi}{2}. \tag{64}$$

Setting $\zeta = \Psi(Z = 0)$, and noticing $\Psi \to 0$ when $Z \to \infty$, it is obtained that

$$\tanh\frac{\Psi}{4} = \mathrm{e}^{-Z\sqrt{c_0}}\tanh\frac{\zeta}{4}. \tag{65}$$

To explicitly give the distribution of zeta potential ζ, we utilize the $\mathcal{O}(1)$ terms of electrostatic interface condition at $Z = 0$ (32) (i.e., $r \to 1_-$)

$$\left.\frac{\partial\Psi}{\partial Z}\right|_{Z=0} = -\sigma \equiv -2\sqrt{c_0}\sinh\frac{\zeta}{2}, \tag{66}$$

which gives a homogeneous zeta potential $\zeta \equiv \zeta_0$. The zeroth-order tangential electric field in the diffuse layer can be calculated

$$\frac{\partial\Phi_0}{\partial\theta} = \frac{\partial\Psi}{\partial\theta} + \left.\frac{\partial\varphi_0}{\partial\theta}\right|_{r=1} = \mathcal{B}\Theta(\theta). \tag{67}$$

For the fluid flow in the inner region, considering the $\mathcal{O}(\delta^{-3})$ terms of the Stokes equation (22) along r-direction, it is derived that

$$\frac{\partial P_{-2}}{\partial Z} = \frac{\partial^2\Psi}{\partial Z^2}\frac{\partial\Psi}{\partial Z}. \tag{68}$$

Taking the integral along Z from Z to ∞, it is obtained that

$$P_{-2} = \frac{1}{2}\left(\frac{\partial\Psi}{\partial Z}\right)^2. \tag{69}$$

Here, we have utilized the properties of $P_{-2} \to 0$ and $\partial\Phi_0/\partial Z \to 0$ when $Z \to \infty$. Then, considering the $\mathcal{O}(\delta^{-2})$ terms of the Stokes equation (22) along θ direction, it is derived that

$$\frac{\partial P_{-2}}{\partial\theta} = \frac{\partial^2 V_0}{\partial Z^2} + \frac{\partial^2\Psi}{\partial Z^2}\frac{\partial\varphi_0}{\partial\theta}, \tag{70}$$

where the pressure gradient can be explicitly calculated

$$\frac{\partial P_{-2}}{\partial\theta} = \frac{\partial\Psi}{\partial Z}\frac{\partial^2\Psi}{\partial Z\partial\theta} = \sinh\Psi\frac{\partial\Psi}{\partial\theta}\left(\equiv -Q_0\frac{\partial\Psi}{\partial\theta}\right). \tag{71}$$

Taking the integral of Equation (70) along Z from Z to ∞, and utilizing the properties of $\Psi \to 0$, $\partial\Psi/\partial Z \to 0$, and $\partial V_0/\partial Z \to 0$ when $Z \to \infty$, it is obtained that

$$\frac{\partial V_0}{\partial Z} = -\frac{\partial\Psi}{\partial Z}\frac{\partial\varphi_0}{\partial\theta}. \tag{72}$$

Doing the integral again from Z to ∞ and noticing that $V_0 \to v_0$ when $Z \to \infty$, it is derived that

$$v_0 - V_0 = \Psi\frac{\partial\varphi_0}{\partial\theta}. \tag{73}$$

Taking advantage of the definition of $\zeta \equiv \Psi(Z = 0)$ at $Z = 0$, we obtain the effective interface condition of velocity

$$v_0 - V_0|_{Z=0} = \zeta\frac{\partial\varphi_0}{\partial\theta} = \mathcal{B}\zeta\Theta(\theta). \tag{74}$$

For solid wall, $V_0|_{Z=0}$ is prescribed and the final velocity boundary can be obtained directly, while for liquid–liquid interface, $V_0|_{Z=0}$ is undetermined, and the shear stress condition is required to obtain the velocity and pressure fields.

Considering the interface condition of shear stress (31), the $\mathcal{O}(\delta^{-1})$ terms gives

$$\frac{\partial V_0}{\partial Z} = \sigma\left.\frac{\partial\varphi_0}{\partial\theta}\right|_{r=1}. \tag{75}$$

In fact, taking $Z = 0$ in Equation (72) and utilizing the electrostatic interface condition (66), we can similarly obtained

$$\frac{\partial V_0}{\partial Z} = -\frac{\partial\Psi}{\partial Z}\left.\frac{\partial\varphi_0}{\partial\theta}\right|_{r=1} \equiv \sigma\left.\frac{\partial\varphi_0}{\partial\theta}\right|_{r=1}. \tag{76}$$

Therefore, the higher-order solution in the inner region is required, that is, to consider the $\mathcal{O}(1)$ terms in the shear stress interface condition

$$\frac{\partial V_1}{\partial Z} - V_0 - \eta_r\left(\frac{\partial\bar{v}}{\partial r} - \bar{v}\right) = \sigma\frac{\partial\varphi_1}{\partial\theta}. \tag{77}$$

To this end, we have to solve the higher-order equations to determine the terms $\partial V_1/\partial Z$ and $\partial v_0/\partial r$ to provide the complete effective interface condition for shear stress matching. In specific, we consider the $\mathcal{O}(\delta^{-2})$ of the Stokes equation (22) along r-direction

$$\begin{aligned}\frac{\partial P_{-1}}{\partial Z} &= \left(2\frac{\partial\Phi_0}{\partial Z}\right)\frac{\partial\Phi_0}{\partial Z} + \left(\frac{\partial^2\Phi_0}{\partial Z^2}\right)\frac{\partial\Phi_1}{\partial Z} + \left(\frac{\partial^2\Phi_1}{\partial Z^2}\right)\frac{\partial\Phi_0}{\partial Z}\\ &= 2\left(\frac{\partial\Phi_0}{\partial Z}\right)^2 + \frac{\partial}{\partial Z}\left(\frac{\partial\Phi_0}{\partial Z}\frac{\partial\Phi_1}{\partial Z}\right).\end{aligned} \tag{78}$$

Note that since the velocity inhomogeneity $\nabla^2\boldsymbol{u}$ can only contribute the order of $\mathcal{O}(\delta^{-1})$, it disappears in the above balance

equation. Taking the integral along Z from Z to ∞ and utilizing $\partial\Phi_1/\partial Z \equiv \partial\Psi/\partial Z$, it is obtained that

$$-P_{-1} = 8\int_Z^\infty \sinh^2\frac{\Psi(Z')}{2}dZ' - \frac{\partial\Psi}{\partial Z}\frac{\partial\Phi_1}{\partial Z}, \tag{79}$$

where the exponential decay property of Ψ when $Z \to \infty$ has been used. Working out the integral, the explicit form of P_{-1} is written as follows:

$$P_{-1} = -16\sinh^2\frac{\Psi}{4} + \frac{\partial\Psi}{\partial Z}\frac{\partial\Phi_1}{\partial Z}. \tag{80}$$

Then, consider the $\mathcal{O}(\delta^{-1})$ terms of the Stokes equation (22) along θ direction

$$\frac{\partial P_{-1}}{\partial\theta} = \frac{\partial^2 V_1}{\partial Z^2} + 2\frac{\partial V_0}{\partial Z} + \left(\frac{\partial^2\Phi_1}{\partial Z^2} + 2\frac{\partial\Psi}{\partial Z}\right)\frac{\partial\varphi_0}{\partial\theta} + \frac{\partial^2\Psi}{\partial Z^2}\left(\frac{\partial\Phi_1}{\partial\theta} - Z\frac{\partial\varphi_0}{\partial\theta}\right), \tag{81}$$

where the first two terms originate from the velocity inhomogeneity $\nabla^2\boldsymbol{u}$, while the last two terms come from $\nabla^2\varphi\nabla\varphi$, in which the linear term of Z results from the $\mathcal{O}(\delta)$ terms in the expansion of $(1/r)\partial/\partial\theta$. Taking the integral along Z from Z to ∞, the explicit from of $\partial V_1/\partial Z$ is obtained

$$\frac{\partial v_0}{\partial r} - \left.\frac{\partial V_1}{\partial Z}\right|_{Z=0} = \zeta\frac{\partial\varphi_0}{\partial\theta} - \sigma\frac{\partial\Phi_1}{\partial\theta} + 2\int_0^\infty \frac{\partial\Psi}{\partial Z}\frac{\partial^2\Phi_1}{\partial Z\partial\theta}dZ. \tag{82}$$

Combining the perturbation form of shear stress (72) and velocity (74), it is finally obtained that

$$\left(\frac{\partial v_0}{\partial r} - v_0\right) - \eta_r\left(\frac{\partial\bar{v}_0}{\partial r} - \bar{v}_0\right) = 2\int_0^\infty \frac{\partial\Psi}{\partial Z}\frac{\partial^2\Phi_1}{\partial Z\partial\theta}dZ. \tag{83}$$

The right-hand-side term is related to the higher-order electric potential field and must be determined in conjunction with the higher-order equations for ion concentration and electric potential, reflecting the effects associated with ion concentration polarization. Following the previous work [10], the approximate solution is written as

$$\frac{\partial\Phi_1}{\partial\theta} = -\frac{\partial c_1}{\partial\theta}\sinh\frac{\Psi}{2}\left(Z + \frac{1}{\cosh(\zeta/2)}\right) + \frac{\partial\varphi_1}{\partial\theta}. \tag{84}$$

Substituting into Equation (83), the final form of effective interface condition of shear stress matching can be obtained as follows after the integral

$$\left(\frac{\partial v_0}{\partial r} - v_0\right) - \eta_r\left(\frac{\partial\bar{v}_0}{\partial r} - \bar{v}_0\right) = -4\frac{\sinh^2(\zeta/4)}{\cosh(\zeta/2)}\frac{\partial c_1}{\partial\theta}. \tag{85}$$

To determine the ion concentration polarization term $\partial c_1/\partial\theta$ in the above equation, it is required to provide the governing equations as well as the boundary conditions for c_1 in the outer region. From the advection–diffusion equation for salt concentration (24) as well as $c_0 \equiv 1$ and $q_0 \equiv 0$, it is obtained that c_1 obeys the following advection–diffusion equation:

$$\nabla^2 c_1 = \mathcal{A}\boldsymbol{u}_0\cdot\nabla c_1, \tag{86}$$

which satisfies the boundary condition at $r \to \infty$

$$c_1 \to 0, \tag{87}$$

and the matching condition at $r = 1$

$$\left.\frac{\partial c_1}{\partial r}\right|_{r=1} = -J_1(Z\to\infty). \tag{88}$$

Here, the normal ionic flux can be given by solving the advection–diffusion equation in the inner region

$$J_1(Z\to\infty) = -6\mathcal{B}\cos\theta\left((1+2\mathcal{A})\sinh\frac{\zeta}{2} - \mathcal{A}\zeta\cosh\frac{\zeta}{2}\right) - \frac{4\mathcal{A}\sinh^2(\zeta/4)}{\sin\theta}\frac{d}{d\theta}(v_0\sin\theta). \tag{89}$$

3.3 | Effective Interfacial Conditions: Incorporating Induced Charge Effect

Here, we will evaluate how the externally induced charge regulate the previous results. It is important to note that this study introduces the breaking of spherical symmetry in the interfacial ζ potential due to induced charges on the dielectric interface under an external field. This will profoundly influence the ion concentration polarization behavior and be incorporated into the tangential velocity boundary, shear stress boundary, and ion flux boundary. Here, σ is recognized as the initial surface charge density contributed by the adsorbed solute ions at interface induced by the interfacial chemical reaction, which may further redistribute under external electric field and fluid convection. It is noteworthy that we ignore the effects of further chemical reactions that possibly regulate the surface charge density.

To explicitly give the distribution of zeta potential ζ, we utilize the electrostatic interface condition at $Z = 0$ (i.e., $r \to 1_-$) [Equation (32)]

$$\left.\frac{\partial\Psi}{\partial Z}\right|_{Z=0} = \varepsilon_r\frac{\partial\bar{\bar{\varphi}}}{\partial r} - \sigma \equiv -2\sqrt{c_0}\sinh\frac{\zeta}{2}. \tag{90}$$

Here, it has been required that the field-induced potential at the dielectric surface satisfies $\bar{\bar{\varphi}} \equiv \delta\bar{\varphi} \ll 1$, which represents a $\mathcal{O}(\delta)$ correction to the $\mathcal{O}(1)$ quantities serving as a modification to the standard expansion [Equation (66)]. The induced potential inside the dielectric droplet $\bar{\varphi}$ is assumed to be approximately given by the permittivity-mismatching condition

$$\bar{\varphi} = \zeta - \frac{3}{2+\varepsilon_r}\mathcal{B}r\cos\theta, \quad 0 < r < 1, \tag{91}$$

which indicates that the aforementioned scaling requirement is equivalent to $\delta\mathcal{B} \ll 1$. Substituting the induced potential distribution into the zeta potential distribution, it is obtained that

$$2\sqrt{c_0}\sinh\frac{\zeta(\theta)}{2} = \sigma + \frac{3\varepsilon_r}{2+\varepsilon_r}\delta\mathcal{B}\cos\theta. \tag{92}$$

Taking the derivatives of both sides, it is derived that

$$\frac{d\zeta}{d\theta} = -\frac{1}{\cosh(\zeta/2)}\mathcal{B}\frac{3\delta\varepsilon_r}{2+\varepsilon_r}\sin\theta \equiv -\frac{1}{\cosh(\zeta/2)}\mathcal{B}\xi_{\delta\varepsilon}\Theta(\theta), \tag{93}$$

where we have noted $\xi_{\delta\varepsilon} \equiv \delta\cdot\varepsilon_r/(1+\varepsilon_r/2)$ and $\Theta(\theta) \equiv (3/2)\sin\theta$, and utilized $c_0 \equiv 1$. Setting $\zeta_0 = 2\sinh^{-1}(\sigma/2)$, the above result can be approximately reduced to the following

when $\zeta \ll 1$

$$\zeta(\theta) = \zeta_0 + \frac{3\varepsilon_r}{2+\varepsilon_r}\delta\mathcal{B}\cos\theta. \tag{94}$$

This result reflects the variation of ζ on θ, which essentially stems from the induced charging effect on dielectric surfaces and the broken spherical symmetry of interfacial charging, and distinguishes the current study from previous work [10]. The *moderate* external field condition requires $\delta\mathcal{B} \ll \zeta_0$ [30, 47], and we will not distinguish ζ from ζ_0 when the $\partial\zeta/\partial\theta$ is unimportant. In fact, by allowing $\delta\mathcal{B} \ll \min\{1, \zeta_0\}$, we expect that the following results may still stand even if $\mathcal{B}$ is not small enough given that $\delta \ll 1$, which, however, still requires further validation by numerical simulations or experiments.

From Equation (65), it is noticed that the arguments of functions Ψ, $C_0 = \cosh\Psi$ and $Q_0 = \sinh\Psi$ can be written in a unified form of $g_1(Z)g_2(\zeta(\theta))$, and the Z-derivatives of those functions $\partial(\cdot)/\partial Z$ are the functions of Ψ itself from Equation (64), whose characteristics are essential for the analytical solutions of the higher-order equations. Accordingly, Equation (67) should be replaced with

$$\frac{\partial\Phi_0}{\partial\theta} = \frac{\partial\Psi}{\partial\theta} + \left.\frac{\partial\varphi_0}{\partial\theta}\right|_{r=1} = -\frac{2\sinh(\Psi/2)}{\sinh\zeta}\mathcal{B}\xi_{\delta\varepsilon}\Theta(\theta) + \mathcal{B}\Theta(\theta). \tag{95}$$

This result is obtained by taking the derivatives of expression of Ψ [Equation (65)], and the result of $d\zeta/d\theta$ has also been utilized. It is indicated that the zeroth-order tangential electric field is no longer uniform along the Z-direction (which is distinct from the gas bubble [10]), where the Z-dependence $\partial\Psi/\partial\theta$ varies in a similar tendency as e^{-Z}. In the scenario considering induced charging on dielectric surfaces, although the total charge of the quasi-equilibrium diffuse layer is zero, the additional tangential electric field generated by inhomogeneous charging will contribute to a nonzero total effective shear stress. This shear stress is of the order of $\mathcal{f}$ under low surface potential conditions, which significantly differs from bubble electrophoresis where induced interfacial charge is neglected [10], but bears some resemblance to the electrocapillary motion behavior of metal droplets [8, 9]. In particular, it is noteworthy noting that in this study we denote $\delta\bar{\varphi}$ as $\tilde{\varphi} = \mathcal{O}(\delta)$, which means the induced charge effect only has a $\mathcal{f}$ contribution as a correction term. This can be seen as a heuristic treatment extending the method of matched asymptotic expansion, which indeed is quite different from those previous studies that treat $\bar{\varphi}_{-1} = \delta\bar{\varphi}$ as a $\mathcal{O}(1)$ quantity under strong fields $\mathcal{B} = \mathcal{O}(\delta^{-1})$ [30, 48].

As for the fluid flow, Equation (72) should be replaced by

$$\frac{\partial V_0}{\partial Z} = \frac{2\sinh^2(\Psi/2)}{\sinh\zeta}\mathcal{B}\xi_{\delta\varepsilon}\Theta(\theta) - \frac{\partial\Psi}{\partial Z}\frac{\partial\varphi_0}{\partial\theta}. \tag{96}$$

Therefore, after a similar operation of integration, it is obtained that

$$v_0 - V_0 = \Psi\frac{\partial\varphi_0}{\partial\theta} + \mathcal{B}\xi_{\delta\varepsilon}\Theta(\theta)\frac{4\sinh^2(\Psi/4)}{\sinh\zeta}. \tag{97}$$

Then, Equation (74) is replaced by

$$\begin{aligned} v_0 - V_0|_{Z=0} &= \zeta\frac{\partial\varphi_0}{\partial\theta} + \mathcal{B}\xi_{\delta\varepsilon}\Theta(\theta)\frac{4\sinh^2(\zeta/4)}{\sinh\zeta}. \\ &= \mathcal{B}\zeta\Theta(\theta) + \mathcal{B}\xi_{\delta\varepsilon}\Theta(\theta)\frac{\tanh(\zeta/4)}{\cosh(\zeta/2)}. \end{aligned} \tag{98}$$

Besides, from Equation (96), it yields

$$\frac{\partial V_0}{\partial Z} = \tilde{\sigma}\left.\frac{\partial\varphi_0}{\partial\theta}\right|_{r=1} + \mathcal{O}(\mathcal{B}^2), \tag{99}$$

which still share the similar formulation to Equation (75), with $\tilde{\sigma} = \sigma + \mathcal{O}(\varepsilon_r\zeta)$ the surface charge density where the induced charge effect has been incorporated [10].

As previously mentioned, determining the leading-order effective interfacial condition for the shear stress at droplet interface and capturing the polarization behavior of nearby ion concentrations require further reliance on higher-order solutions within the inner region. Specifically, the former necessitates the use of the momentum equation incorporating higher-order pressure terms to provide the shear stress matching at the interface, while the latter requires solving for higher-order electric potential and ion concentrations to establish the boundary conditions for the higher-order ion concentration field.

For the former one, to obtain the shear stress boundary, Equation (82) is replaced by

$$\begin{aligned} \left.\frac{\partial v_0}{\partial r} - \frac{\partial V_1}{\partial Z}\right|_{Z=0} &= 4\mathcal{B}\xi_{\delta\varepsilon}\Theta(\theta)\frac{\tanh(\zeta/4)}{\cosh(\zeta/2)} + \zeta\frac{\partial\varphi_0}{\partial\theta} - \tilde{\sigma}\frac{\partial\Phi_1}{\partial\theta} \\ &\quad + 2\int_0^\infty \frac{\partial\Psi}{\partial Z}\frac{\partial^2\Phi_1}{\partial Z\partial\theta}dZ. \end{aligned} \tag{100}$$

The detailed derivation of Equation (100) can be found in Appendix A.1. Then, Equation (83) should be replaced by

$$\begin{aligned} \left(\frac{\partial v_0}{\partial r} - v_0\right) - \eta_r\left(\frac{\partial\bar{v}_0}{\partial r} - \bar{v}_0\right) &= 3\mathcal{B}\xi_{\delta\varepsilon}\Theta(\theta)\frac{\tanh(\zeta/4)}{\cosh(\zeta/2)} \\ &\quad + 2\int_0^\infty \frac{\partial\Psi}{\partial Z}\frac{\partial^2\Phi_1}{\partial Z\partial\theta}dZ. \end{aligned} \tag{101}$$

The additional first term on the right-hand side of the equation is explicitly expressed, representing the contribution of the normal nonuniform electric field induced by charges on the dielectric surface. Solving the higher-order electric potential and concentration fields, Equation (84) is replaced by

$$\frac{\partial\Phi_1}{\partial\theta} = -\left(\frac{\partial c_1}{\partial\theta} - \frac{2\mathcal{B}\xi_{\delta\varepsilon}\Theta(\theta)}{\sinh\zeta}\right)\sinh\frac{\Psi}{2}\left(Z + \frac{1}{\cosh(\zeta/2)}\right) + \frac{\partial\varphi_1}{\partial\theta}. \tag{102}$$

Thus, the shear stress matching condition is modified as follows:

$$\begin{aligned} &\left(\frac{\partial v_0}{\partial r} - v_0\right) - \eta_r\left(\frac{\partial\bar{v}_0}{\partial r} - \bar{v}_0\right) \\ &= \mathcal{B}\xi_{\delta\varepsilon}\Theta(\theta)\frac{\tanh(\zeta/4)}{\cosh(\zeta/2)}\left(3 + \frac{2}{\cosh(\zeta/2)}\right) - 4\frac{\sinh^2(\zeta/4)}{\cosh(\zeta/2)}\frac{\partial c_1}{\partial\theta}. \end{aligned} \tag{103}$$

The detailed derivation of Equations (102) and (103) can be found in Appendix A.2.

For the latter one, the ionic flux boundary [Equation (89)] is accordingly replaced by

$$J_1(Z\to\infty) = -6\mathcal{B}\cos\theta\left((1+2\mathcal{A})\sinh\frac{\zeta}{2}-\mathcal{A}\zeta\cosh\frac{\zeta}{2}\right) + 3\xi_{\delta\varepsilon}\mathcal{B}\cos\theta\left(\tanh\frac{\zeta}{2}+\mathcal{A}\frac{2\tanh(\zeta/4)\sinh^2(\zeta/4)}{\cosh(\zeta/2)}\right) - \frac{4\mathcal{A}\sinh^2(\zeta/4)}{\sin\theta}\frac{d}{d\theta}(v_0\sin\theta). \tag{104}$$

The detailed derivation of Equation (104) can be found in Appendix A.3.

4 | Results and Discussions

In this section, we will first organize the formulation of the outer region boundary value problem obtained through the coarse-grained method of matched asymptotic expansions from the previous section and discuss its physical significance. Then, under specific parameter limits, we will provide its analytical solution and explore the mechanisms of ion concentration polarization effects. As an application of the analytical solutions, this section will also incorporate the large viscosity ratio assumption to develop a charging mechanism model based on the dependence of electrophoretic mobility on pH and discuss its physical implications.

4.1 | Recapitulation of Coarse-Grained Problem and Brief Discussion

Taking the thin double layer limit $\delta\to 0$, rewriting c_1 as c, and utilizing φ and $\boldsymbol{u}$ to denote the leading-order terms, we can organize the coarse-grained problems in the outer regions outside the diffuse layer region. Note that, the terms with coefficient $\xi_{\delta\varepsilon}$ represent the correction by induced charge effect.

The coarse-grained governing equation for salt concentration field c is

$$\nabla^2 c = \mathcal{A}\boldsymbol{u}\cdot\nabla c, \quad r>1, \tag{105}$$

which satisfies the normal salt flux boundary condition at $r=1$

$$\frac{\partial c}{\partial r} = 6\mathcal{B}\cos\theta\left((1+2\mathcal{A})\sinh\frac{\zeta}{2}-\mathcal{A}\zeta\cosh\frac{\zeta}{2}\right) - 3\xi_{\delta\varepsilon}\mathcal{B}\cos\theta\left(\tanh\frac{\zeta}{2}+\mathcal{A}\frac{2\tanh(\zeta/4)\sinh^2(\zeta/4)}{\cosh(\zeta/2)}\right) + \frac{4\mathcal{A}\sinh^2(\zeta/4)}{\sin\theta}\frac{d}{d\theta}(v\sin\theta) \equiv 6\mathcal{B}\cos\theta\mathcal{Z}_1(\zeta)+\frac{\mathcal{Z}_2(\zeta)}{\sin\theta}\frac{d}{d\theta}(v\sin\theta). \tag{106}$$

Here, $\mathcal{Z}_1=\mathcal{O}(\zeta)$ and $\mathcal{Z}_2=\mathcal{O}(\zeta^2)$ (for $\zeta\to 0$). The boundary condition at $r\to\infty$ is written as

$$c\to 0. \tag{107}$$

The coarse-grained governing equations for velocity and pressure fields $\boldsymbol{u}$ ($\bar{\boldsymbol{u}}$) and p ($\bar{p}$) are

$$\nabla\cdot\boldsymbol{u}=0, \quad \nabla p=\nabla^2\boldsymbol{u}, \quad r>1 \tag{108}$$

$$\nabla\cdot\bar{\boldsymbol{u}}=0, \quad \nabla\bar{p}=\eta_r\nabla^2\bar{\boldsymbol{u}}, \quad 0<r<1, \tag{109}$$

which satisfies the normal impenetrability condition at $r=1$

$$u=\bar{u}=0, \tag{110}$$

the tangential velocity jump condition at $r=1$

$$v-\bar{v}=\mathcal{B}\Theta(\theta)\left(\zeta-\xi_{\delta\varepsilon}\frac{\tanh(\zeta/4)}{\cosh(\zeta/2)}\right)\equiv\mathcal{B}\Theta(\theta)\mathcal{Z}_3(\zeta), \tag{111}$$

where $\mathcal{Z}_3=\mathcal{O}(\zeta)$ (for $\zeta\ll 1$), and the shear stress matching condition at $r=1$

$$\left(\frac{\partial v}{\partial r}-v\right)-\eta_r\left(\frac{\partial\bar{v}}{\partial r}-\bar{v}\right) = \mathcal{B}\xi_{\delta\varepsilon}\Theta(\theta)\frac{\tanh(\zeta/4)}{\cosh(\zeta/2)}\left(3+\frac{2}{\cosh(\zeta/2)}\right)-4\frac{\sinh^2(\zeta/4)}{\cosh(\zeta/2)}\frac{\partial c}{\partial\theta} \equiv\mathcal{B}\Theta(\theta)\mathcal{Z}_4(\zeta)-\frac{\partial c}{\partial\theta}\mathcal{Z}_5(\zeta), \tag{112}$$

where $\mathcal{Z}_4=\mathcal{O}(\zeta)$ and $\mathcal{Z}_5=\mathcal{O}(\zeta^2)$ (for $\zeta\to 0$). The boundary condition at $r\to\infty$ is written as

$$u\to-\mathcal{U}\cos\theta, \quad v\to\mathcal{U}\sin\theta. \tag{113}$$

To make the problem physically meaningful, it should also satisfy the finite velocity condition at $r=0$

$$\bar{u},\bar{v}<\infty. \tag{114}$$

The problem is finally enclosed by the force balance condition of droplet

$$\oint_{r=1}\left(-p\boldsymbol{I}+(\nabla\boldsymbol{u}+(\nabla\boldsymbol{u})^T)\right)\cdot\boldsymbol{e}_r dA=0. \tag{115}$$

Based on the above theoretical formulation of the coarse-grained problem for electrophoresis of dielectric droplets, a preliminary discussion of the transport mechanism in the outer regions outside the electric double layer can be conducted as follows.

1. From the perspective of multiphysics coupling, the concentration field and the velocity field are mutually coupled through the boundary conditions at the interface $r=1$. Here, the velocity field primarily influences the concentration field via interfacial convective transport, while the concentration field affects the velocity field mainly by inducing nonuniform osmotic pressure at the interface, corresponding to the convection-induced ion concentration polarization effect. The characteristic coupling coefficients $\mathcal{Z}_2$ and $\mathcal{Z}_5$ for these interactions are both of the order $\mathcal{O}(\zeta^2)$. In this study, by introducing the induced charge effect, the contribution of inhomogeneous interfacial charging to the ion concentration polarization effect is further considered, with its characteristic coefficients $\mathcal{Z}_1$ and $\mathcal{Z}_4$ being of the order $\mathcal{O}(\zeta)$. These results imply that under low surface potential conditions,

the linear terms of the external electric field and the induced tangential electric field dominate, whereas under high surface potential conditions, the nonlinear terms of interfacial convection and diffusive permeation play a major role. Notably, although the derivation involves the higher-order potential fields Φ_1 and φ_1 within the electric double layer and at its outer edge, the final formulation does not include the perturbation of the higher-order potential field φ_1. This outcome primarily stems from the highest-order term in the scaling analysis of the Stokes momentum equation (22), which is determined by the velocity field's magnitude confirmed by the stress boundary condition (31). In addition, if the shape change of the droplet during electrophoresis is minimal, its normal deformation can be determined through the normal stress matching condition at the droplet surface $r = 1$ and is related to Ca [9, 42].

2. From the perspective of control parameter effects, the external electric field strength $\mathcal{B}$ acts linearly in the ion concentration flux boundary, tangential velocity jump condition, and tangential stress matching condition at $r = 1$. On the other hand, the influence of the interfacial ζ potential is closely related to the magnitude of the dynamic viscosity ratio η_r and the dielectric constant ratio ε_r. When η_r is nonnegligible, the characteristic velocity $\mathcal{U}$ needs to be determined by simultaneously solving the tangential velocity jump condition and the tangential stress matching condition. Its magnitude under low surface potential ζ conditions is governed by the velocity boundary and can be estimated as $\mathcal{O}(\zeta)$. In this case, the ion concentration polarization effect in the tangential stress matching becomes significant primarily under high dielectric constant ratio $\varepsilon_r \gtrsim 1$ and high surface potential $\zeta \gtrsim 1$ conditions, while it only constitutes a minor correction to the original result under low surface potential ζ. When $\eta_r \to 0$, the magnitude of the characteristic velocity $\mathcal{U}$ can be estimated through the tangential stress matching condition, and the discussion is divided based on the magnitude of the parameter ζ. For the low surface potential case where $\zeta \ll 1$, if $\varepsilon_r \neq 0$, the $\mathcal{Z}_4$ term is the leading-order term with respect to ζ, and the electrophoretic velocity is of order $\mathcal{O}(\zeta)$; whereas if $\varepsilon_r \ll 0$, the $\mathcal{Z}_5$ term becomes the leading-order term, and the electrophoretic velocity is of order $\mathcal{O}(\zeta^3)$. For the high surface potential case where $\zeta \gtrsim 1$, the characteristic coefficient $\mathcal{Z}_4$ for interfacial induced inhomogeneous charging tends to 0, while the characteristic coefficients $\mathcal{Z}_1$ and $\mathcal{Z}_2$ for ion convective concentration polarization exhibit significant nonlinear effects with respect to ζ. Consequently, the characteristic coefficient $\mathcal{Z}_5$ for the interfacial diffusive permeation effect is of order $\mathcal{O}(1)$. In addition, for the hydrodynamic viscous coupling coefficient $\mathcal{A}$ of ions, it primarily influences ion transport behavior through the convective diffusion equation and the convective term of the concentration normal flux at the $r = 1$ boundary, where the characteristic coefficient at the normal flux boundary is related to the excess ion concentration $\mathcal{Z}_2$ at the interface. However, even if $\mathcal{A} \to 0$, the ion concentration distribution may still enter the normal flux boundary due to the action of the external electric field $\mathcal{B}$, thereby triggering ion concentration polarization behavior.

3. From the perspective of comparing different systems, when $\eta_r \to \infty$, the order-of-magnitude estimation of the aforementioned tangential stress matching condition will yield $\bar{v} = 0$. In this case, the problem reduces to the tangential velocity jump condition, leading to the same conclusion as for solid particles, an inference that can be verified by the analytical solution form presented below. When $\eta_r \to 0$, the results for the electrophoresis of bubbles are obtained. Particularly, since bubbles generally satisfy $\varepsilon_r \to 0$, the aforementioned boundary value problem will reduce to the expression found in previous studies on bubble electrophoresis [10]. In previous research, it was common to directly set $\eta_r = \varepsilon_r = 0$, which results in the characteristic velocity $\mathcal{U}$ being determined solely by the $\mathcal{O}(\zeta^3)$ term related to ion concentration polarization in the tangential stress matching condition. This can partially explain why previous studies obtained a zero electrophoretic velocity for bubbles under low surface potential $\zeta \ll 1$ conditions using a linear expansion in ζ. However, the derivation in this paper shows that the nonlinear dependence of electrophoretic velocity on ζ at low surface potentials and the linear dependence on the small parameters $\eta_r, \varepsilon_r \ll 1$ are difficult to distinguish, necessitating further estimation of the influence of small parameter magnitudes. As for metal droplets, there are no stresses other than viscous forces within their interface and interior that balance the electric double layer electric field forces, which makes the order-of-magnitude estimation of the velocity field via stress boundary conditions significantly different from that of dielectric droplets [9, 43]. In this scenario, the final form of the boundary value problem will be expressed in terms of the higher-order potential field φ_1 rather than the higher-order concentration field c_1, which is consistent with the physical picture of metal droplets exhibiting significant induced charging effects under an external electric field.

4.2 | Closed-Form Analytical Solution Under Several Parameter Limits

In the zero-divergence condition of stress tensor, the stream functions on both sides of spherical surfaces can be directly written down as follows [49]:

$$\psi = -\frac{1}{2}\mathcal{U}\left(r^2 - \frac{1}{r}\right)\sin^2\theta, \quad r > 1 \tag{116}$$

$$\bar{\psi} = -\frac{3}{4}\bar{\mathcal{U}}\left(r^4 - r^2\right)\sin^2\theta, \quad 0 < r < 1, \tag{117}$$

the latter of which corresponds to the Hill's spherical vortex. The above stream functions will lead to the following velocity fields in the outer regions:

$$u = -\mathcal{U}\left(1 - \frac{1}{r^3}\right)\cos\theta, \tag{118}$$

$$v = \mathcal{U}\left(1 + \frac{1}{2r^3}\right)\sin\theta, \tag{119}$$

$$\bar{u} = -\frac{3}{2}\bar{\mathcal{U}}\left(r^2 - 1\right)\cos\theta, \tag{120}$$

$$\bar{v} = 3\bar{\mathcal{U}}\left(r^2 - \frac{1}{2}\right)\sin\theta. \tag{121}$$

The boundary condition at infinity $r \to \infty$, the finite velocity condition at $r = 0$, the zero-divergence condition of stress tensor,

and the normal impenetrability condition at $r = 1$ have been naturally satisfied. To determine the parameters $\mathcal{U}$ and $\bar{\mathcal{U}}$, it is required to utilize the tangential velocity jump condition and shear stress matching condition at $r = 1$, as well as the normal salt flux at $r = 1$ for the salt concentration field. In particular, the following analytical solution will mainly include the concentration solution to the Laplace equation as follows:

$$\nabla^2 c = 0, \quad r > 1, \tag{122}$$

whose nontrivial general solution that is consistent with the dipole boundary condition is written as

$$c = \mathcal{W}\frac{\cos\theta}{r^2}. \tag{123}$$

In the limit of low surface potential $\zeta \ll 1$, the characteristic coupling coefficients are evaluated as

$$\mathcal{Z}_1 = \left(1 - \frac{3}{2}\xi_{\delta\varepsilon}\right)\zeta + \mathcal{AO}(\zeta^3) + o(\zeta^3), \tag{124}$$

$$\mathcal{Z}_2 = \mathcal{AO}(\zeta^2) = o(\zeta), \tag{125}$$

$$\mathcal{Z}_3 = \left(1 - \frac{\xi_{\delta\varepsilon}}{4}\right)\zeta + o(\zeta), \tag{126}$$

$$\mathcal{Z}_4 = \frac{5}{4}\xi_{\delta\varepsilon}\zeta + o(\zeta), \tag{127}$$

$$\mathcal{Z}_5 = \mathcal{O}(\zeta^2) = o(\zeta). \tag{128}$$

Therefore, the normal salt flux at $r = 1$ is of order $\mathcal{O}(\zeta)$, and the tangential velocity jump as well as the shear stress is also of order $\mathcal{O}(\zeta)$. It is then reasonable to conduct the rescaling for $\boldsymbol{u}$ and c into $\boldsymbol{u} = \delta\tilde{\boldsymbol{u}}$ and $c = \delta\tilde{c}$, where the rescaled concentration field $\tilde{c}$ will satisfy the aforementioned Laplace equation. Substituting the interface conditions [Equations (106), (111), and (112)], the undetermined parameters can be solved

$$\mathcal{U} = \mathcal{B}\zeta\frac{3\eta_r(1 - \xi_{\delta\varepsilon}/4) - (5\xi_{\delta\varepsilon}/4)}{3\eta_r + 2}. \tag{129}$$

It is readily observed that the expression reduces to the Smoluchowski formula for the electrophoresis of solid particles when $\eta_r \to \infty$, and to the Booth's solution [20] when $\xi_{\delta\varepsilon} \to 0$. Both of these existing analytical solutions mentioned here rely on the low surface potential condition, which is compatible with the assumptions made herein. Our result is qualitatively consistent with the experimental results of Marinova et al. [4], which show that the droplet electrophoretic mobility increases with the viscosity ratio under same chemical environment setup. Besides, it is a natural question that whether the term $3\eta_r\,[1 - \xi_{\delta\varepsilon}(\varepsilon_r)/4] - [5\xi_{\delta\varepsilon}(\varepsilon_r)/4]$ could be negative which will deduce a quite counterintuitive result the positively charged droplet will move to the reverse direction of the imposed electric field. Figure 3 presents a distribution map of typical oil-to-aqueous solution property ratios, demonstrating that even for relatively thick electric double layers ($\delta \lesssim 1$), the aforementioned term is positive in general.

In the limit of a weak external electric field $\mathcal{B} \ll 1$, the magnitudes of the concentration field c and the velocity field $\boldsymbol{u}$ can

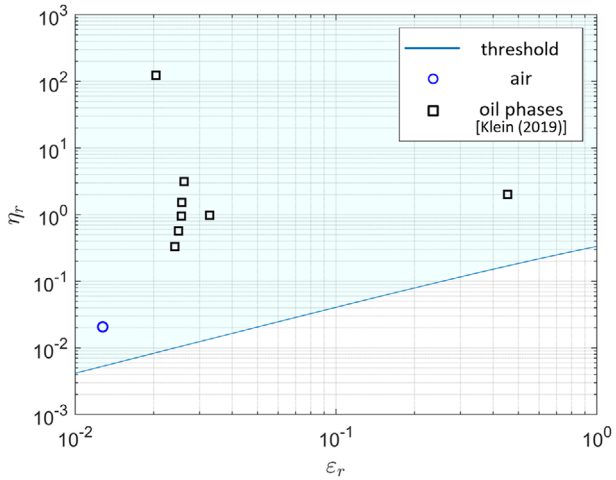

FIGURE 3 | The distribution of the typical nonaqueous phase property ratios η_r and $\xi_{\delta\varepsilon}$, from left to right, includes air, paraffin oil, octane, decane, dodecane, hexadecane, xylene, and nitrobenzene. The experimental data are measurements taken at atmospheric pressure and a temperature of 25°C [4, 50–52]. Among these, the threshold curve corresponds to $3\eta_r\,[1 - \xi_{\delta\varepsilon}(\varepsilon_r)/4] = 5\xi_{\delta\varepsilon}(\varepsilon_r)/4$, where the parameter value $\delta = 1$ has been taken as the limiting case.

similarly be estimated as $\mathcal{O}(\mathcal{B})$. Consequently, scaling transformations are applied to $\boldsymbol{u}$ and c as $\boldsymbol{u} = \mathcal{B}\tilde{\boldsymbol{u}}$ and $c = \mathcal{B}\tilde{c}$, respectively. Under these transformations, the concentration field $\tilde{c}$ satisfies the Laplace equation, making the aforementioned general solution applicable. By substituting the interface conditions (106), (111), and (112) in a similar manner and solving the system of equations, we obtain

$$\mathcal{U} = \mathcal{B}\frac{3\eta_r\mathcal{Z}_3 - \mathcal{Z}_4 + 2\mathcal{Z}_1\mathcal{Z}_5}{3\eta_r + 2 + \mathcal{Z}_2\mathcal{Z}_5}. \tag{130}$$

It is straightforward to verify that this expression reduces to the result under the low surface potential limit as $\zeta \to 0$, while it itself is also applicable to higher surface potential ζ scenarios that may induce significant ion concentration polarization, marking an important contribution of this study that distinguishes it from previous works. Figure 4 illustrates the dependence of $\mathcal{U}$ on ζ for different viscosity ratio η_r parameters. Among these, under low viscosity ratio conditions, a ζ^3 scaling relationship is satisfied at low surface potentials ζ, while under high viscosity ratio conditions, a linear scaling relationship is satisfied at low surface potentials ζ. At higher ζ, all viscosity ratio scenarios exhibit a nonmonotonic dependence on ζ, which is precisely the result of ion concentration polarization. This study is the first to capture the nonmonotonic dependence of electrophoretic mobility on surface charge in the form of an analytical solution, which is qualitatively consistent with previous numerical results where the more complex adsorption kinetic behaviors are included [6].

In fact, using the spectral method based on the associated Legendre functions and with governing equation of c linearized, the higher-order effect of $\xi_{\delta\varepsilon}\mathcal{B}$ in Equations (111), (112), and (106) could be evaluated. Since the force expression is only related to the leading-order Legendre modes of c and $\boldsymbol{u}$, the solution procedure is similar to that in the previous literature [48], and the final electrophoretic velocity expression is similar to Equation (130), with $\mathcal{Z}_{i,0} \equiv \mathcal{Z}_i(\zeta)|_{\zeta=\zeta_0}$ as the leading-order approx-

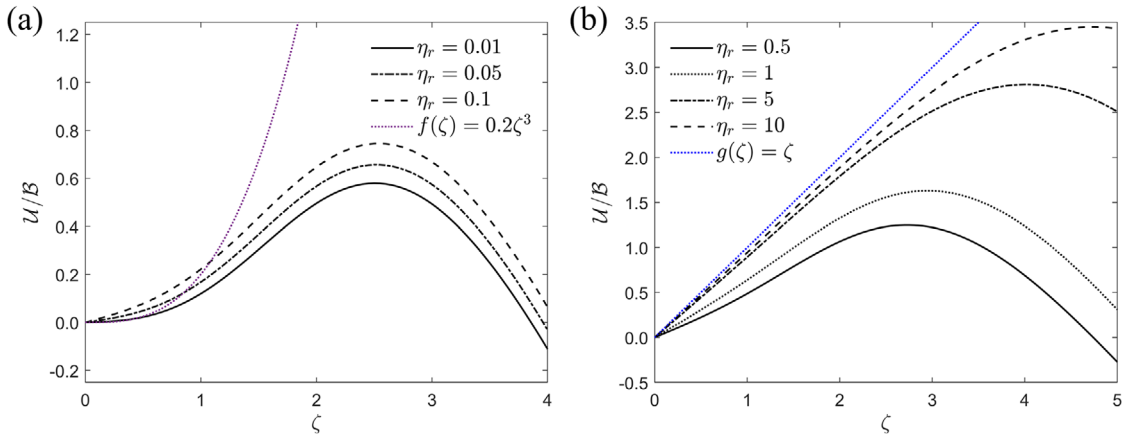

FIGURE 4 | The dependence of the electrophoretic velocity of dielectric droplets on the interfacial ζ potential under different viscosity ratios. (a) Under low viscosity ratio conditions, the low surface potential ζ satisfies the ζ^3 scaling relationship; (b) Under high viscosity ratio conditions, the low surface potential ζ satisfies a linear scaling relationship. At higher ζ values, all viscosity ratio scenarios exhibit a nonmonotonic dependence on ζ.

imation replaced by the moments of polar-angle-dependent quantity $\mathcal{Z}_{i,1} = \mathcal{Z}_{i,1}(\zeta(\zeta_0, \xi_{\delta\varepsilon}\mathcal{B}))$, whose definitions are given as

$$\mathcal{Z}_{i,1} = \frac{\int_0^\pi \mathcal{Z}_i(\zeta(\xi_{\delta\varepsilon}\mathcal{B}, \cos\theta))\cos^2\theta\sin\theta d\theta}{\int_0^\pi \cos^2\theta\sin\theta d\theta}, \tag{131}$$

and

$$\mathcal{Z}_{j,1} = \frac{\int_0^\pi \mathcal{Z}_j(\zeta(\xi_{\delta\varepsilon}\mathcal{B}, \cos\theta))\sin^3\theta d\theta}{\int_0^\pi \sin^3\theta d\theta}, \tag{132}$$

where $i = 1, 2$ and $j = 3, 4, 5$. For simplicity, the detailed result will not be covered in this work. From the formulation, it is straightforward that if the viscosity ratio is set to infinity and concentration effect are ignored, the final electrophoretic velocity expression will reduce to the modified Smoluchowski formula proposed by Schnitzer and Yariv [48].

4.3 | Discussion: Charging Mechanism Model of Nonpolar Oil

For dielectric droplet surfaces composed of nonpolar oils, previous spectroscopic experimental characterizations and molecular dynamics simulation results indicate that the hydrogen bond network near the interface may provide adsorption sites for hydroxide ions. However, (hydrated) hydrogen ions are likely to be closer to the Gibbs interface at the nonpolar oil–water interface than hydroxide ions [53–55]. This seemingly contradictory result can be explained using a triple-layer model as illustrated in Figure 5a. In fact, numerous electrophoresis experiments on inert hydrophobic phases and the two-phase streaming potential experiments from the previous chapter both demonstrate that the contribution of hydroxide ions to the effective interfacial charge, which determines electrokinetic transport, is greater. This results in a negative ζ potential at the nonpolar oil–water interface. To provide a quantitative modeling of the charging mechanism of nonpolar oils, a more straightforward and concise triple-layer model is adopted here, in contrast to the previous quadruple-layer model and surface conductivity correction model. It should be noted that, to highlight the differences from other existing charging models, the large viscosity ratio assumption is applied when obtaining the interfacial ζ potential from droplet electrophoretic mobility, under which the aforementioned electrophoretic analytical solution reduces to the Smoluchowski formula. The experimental measurements of the interfacial ζ potential for the corresponding different nonpolar phases under varying pH conditions can be then obtained, as shown in Figure 5.

TABLE 1 | Parameter comparison between the model of this study and previous charge mechanism models.

	PHREEQCv3 [59]	Bonto et al. [60]	Present model
$\lg K_1$	8.93	−6.23	−3.6
$\lg K_{Na^+}$	0	0.53	0
$\lg K_{Ca^{2+}}$	3.08	1.63	1.5

The mathematical description of the electrical triple-layer (ETL) model and the verification of the solution algorithm can be found in Appendix B. Here, the focus is on comparing model parameters and elucidating the core physical picture. In the model presented in this paper, the saturation adsorption density of hydroxide ions at the interface is $\Gamma_{OH-,\max} = 1/17\ \mathrm{nm}^{-2}$, primarily referencing the work of Marinova et al. [4]; other parameters involved are fitting parameters for the interfacial capacitance, with values of $C_1 = 3.098\ \mathrm{F/m}^{-2}$ and $C_2 = 2.25\ \mathrm{F/m}^{-2}$. Table 1 compares the interfacial reaction equilibrium parameters of different theoretical models, noting that the work of Lützenkirchen et al. [58], which employs a more complex quadruple-layer model, is not listed due to a lack of comparability. As shown in Figure 5b, the results indicate that the simple model selected for this study can provide a more accurate description of the charging at nonpolar oil interfaces, which mainly stems from the inaccurate selection of the saturation adsorption density parameter for hydroxide ions in previous models.

To more clearly understand the physical significance of the aforementioned saturation adsorption density results for hydroxide ions, one can express the corresponding Stern-type adsorption

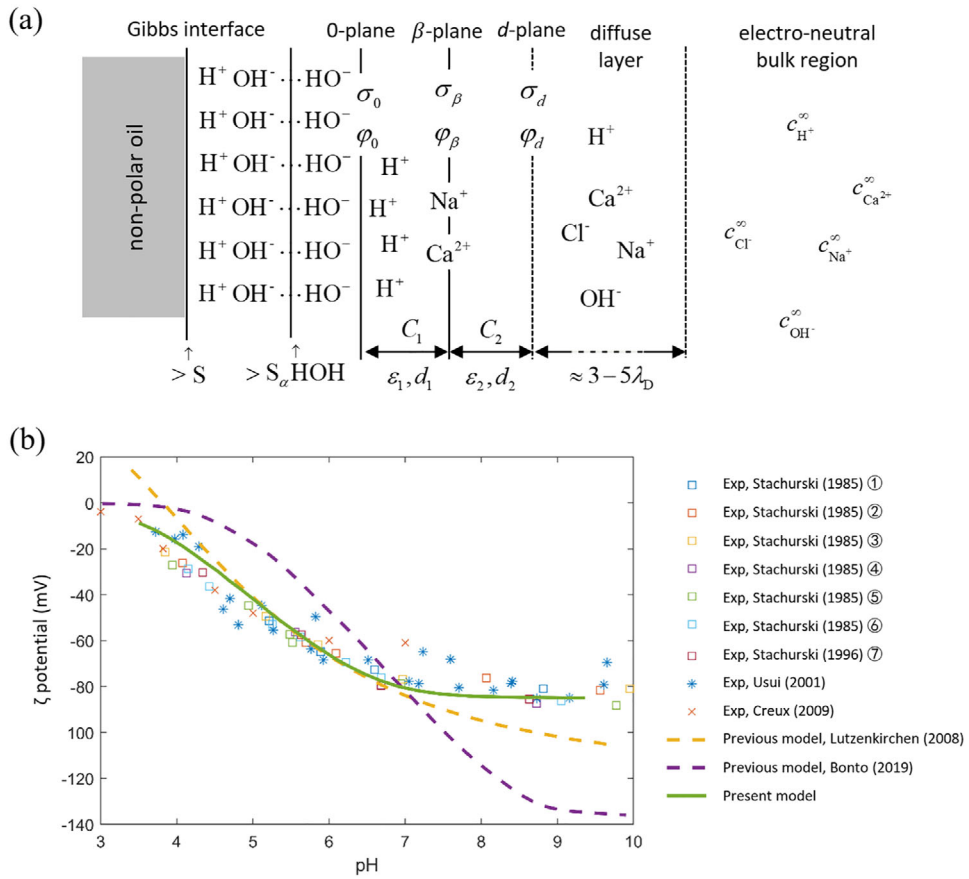

FIGURE 5 | (a) Physical illustration and (b) model validation of surface charging in nonpolar oils. The inert hydrophobic phases used in previous droplet (or bubble) electrophoresis experiments, listed from top to bottom, include nonane (C_9H_{20}), decane ($C_{10}H_{22}$), dodecane ($C_{12}H_{26}$), tridecane ($C_{13}H_{28}$), tetradecane ($C_{14}H_{30}$), octadecane ($C_{18}H_{38}$) (all the aforementioned data are from the same reference [39]), tridecane ($C_{13}H_{28}$) [56], hexacosanol ($C_{26}H_{53}OH$) [57], and nitrogen [40]. The supporting ions in the experiments were derived from 1:1 electrolytes such as NaCl or KCl; the data for nitrogen were measured in the absence of supporting electrolyte ions, while the rest were measured at a supporting electrolyte ion concentration of 1 mM.

isotherm [4] as follows:

$$\frac{\Gamma_{>\text{S-OH}^-}}{\Gamma_{>\text{S-OH}^-,\max}} = \frac{x^{\infty}_{\text{OH}^-}\exp\left(-\frac{\Delta g_a + z_{\text{OH}^-}e\varphi_s}{k_BT}\right)}{1 + x^{\infty}_{\text{OH}^-}\exp\left(-\frac{\Delta g_a + z_{\text{OH}^-}e\varphi_s}{k_BT}\right)}, \tag{133}$$

where Δg_a represents the effective adsorption-free energy of hydroxide ions at the interface. Simultaneously, in the absence of high-valent cations, the effective interfacial adsorption reaction satisfied by hydroxide ions can be phenomenologically written as

$$> S + OH^- \leftrightarrow > S\text{-}OH^-, \tag{134}$$

with the chemical equilibrium constant taking the form

$$K^{\text{eq}} = \frac{\Gamma_{>S\text{-}OH^-}}{\Gamma_{>S}}\frac{1}{c^{\infty}_{OH^-}\exp\left(-z_{OH^-}e\varphi_s/k_BT\right)}. \tag{135}$$

This constant can be related both to the effective adsorption-free energy Δg_a in the adsorption isotherm

$$K^{\text{eq}}c^{\infty}_{OH^-} = x^{\infty}_{OH^-}\exp\left(\frac{\Delta g_a}{k_BT}\right), \tag{136}$$

and to the equilibrium constant K_1 of this model through the ion product of water $K_w = c^{\infty}_{H^+}c^{\infty}_{OH^-}$

$$K_w = K_1K^{\text{eq}}. \tag{137}$$

This implies that the K_1 value obtained from the model fitting can be used to deduce that Δg_a is approximately on the order of $-25k_BT$. Quantitative estimates of intermolecular forces indicate that the binding energy of a single hydroxide ion corresponding to hydrogen bonds is also approximately on the order of $-10\,k_BT\cdot 2 \simeq -20k_BT$ [61], which aligns with the aforementioned hydrogen bond network formation mechanism for hydroxide ion adsorption.

Finally, a brief discussion is provided regarding the assumption of a large viscosity ratio between the droplet and the surrounding solution adopted in the above process. It can be readily observed that when considering a finite viscosity ratio between the droplet and the solution, the same experimentally measured electrophoretic mobility $\mathcal{U}/\mathcal{E}$ would correspond to a higher interfacial ζ potential. From a *qualitative* perspective, for nonpolar phases with different viscosities (as shown in Figure 3), the maximum value and its position of the perturbative solution for droplet electrophoretic mobility increase with viscosity (Figure 4). This qualitatively agrees with the experimental results [4], where the electrophoretic mobility of droplets exhibited a positive correlation with droplet viscosity under identical solution conditions. However, in Figure 5b, the pH-dependent electrophoretic mobility curves reported by Stachurski et al. showed almost no dependence on droplet viscosity. This

discrepancy may reflect the possible influence of surfactant impurities introduced during emulsion preparation. In fact, it has been systematically discussed early on the importance of special purification procedures to remove impurities [4], whereas earlier studies did not mention such treatments [39, 56], suggesting that residual surfactant impurities in their systems might have masked the intrinsic effect of droplet viscosity.

From a *quantitative* standpoint, the maximum electrophoretic mobility measured in Marinova et al.'s experiments roughly ranged between 3.5 and 4. However, given that the viscosity ratios of their nonpolar phases varied from 0.5 to 5, the perturbative solution predicts mobilities only between 1 and 3. This discrepancy may arise from limitations in either the theoretical modeling or its solution procedure. The former includes neglected effects such as droplet deformation from spherical shape, interfacial adsorption kinetics, and tangential ion mobility at the interface [6, 34], while the latter involves approximations like the omission of surface conduction under finite diffuse layer thickness and the higher-order concentration field approximation for ion flux integration. Recently, Hill's work explored the role of finite ion adsorption kinetics and found that if interfacial charges are partially immobilized, the mobility curve versus ζ can be altered (e.g., eliminating the nonmonotonic peak) [34]. The model presented in our work assumes instantaneous equilibrium and fully mobile charges, effectively the limit of infinite interfacial charge diffusivity. It is indicated by Hill that including finite charge transfer or immobilization could potentially reduce the peak mobility and explain why some experiments show a more monotonic behavior [4]. To further verify the theoretical model and verify the solution method, future work should involve numerical solutions based on more comprehensive macroscopic models.

5 | Conclusions and Perspectives

Droplet electrophoresis is one of the most commonly used methods for measuring the charge at nonpolar oil–water interfaces. However, there is still a lack of analytical solutions that consider the ion concentration polarization mechanism under high charge conditions. The main challenges lie in the nonlinear characteristics caused by multiphysical coupled transport near the interface and the complexity of solving the problem due to the finite viscosity ratio and dielectric constant ratio of dielectric droplets. In this study, the matched asymptotic expansion method (including the corresponding heuristic treatment) is employed to derive an analytical solution for dielectric droplet electrophoresis, which is applicable to scenarios with high surface charge and moderate external electric fields. By introducing effective interfacial conditions such as concentration flux boundary, velocity slip boundary, and tangential stress matching conditions, the ion concentration polarization effect, permittivity-induced charge effect, and their coupling mechanism can be effectively captured.

Under low surface potential limit, the analytical solution can be explicitly obtained, which reduces to the Smoluchowski solution for solid particle electrophoresis in the limit of large viscosity ratio, and to the Booth solution in the limit of small dielectric constant ratio. Under weak external electric field limit, the nonmonotonic dependence of the electrophoretic mobility of dielectric droplets on the surface ζ potential is captured for the first time in a closed form of an analytical solution, which is also a typical result of ion concentration polarization. As an application of the analytical solution under high viscosity ratio conditions, quantitative modeling of the adsorption charging mechanism of nonpolar oil is conducted based on previous experimental measurements of droplet electrophoresis. Compared to previous models, the model proposed in this study exhibits better agreement with experimental data over a wider pH range, while offering clearer physical insights and a more concise formulation.

To facilitate future research, numerical solutions of both the full nonlinear macroscopic model and the coarse-grained effective model are strongly recommended. These solutions are essential to verify the asymptotic results and to investigate nonlinear electrophoresis in dielectric droplets. Key numerical challenges include the high computational cost arising from scale disparities at soft interfaces and the issues of numerical stability caused by strong multiphysics coupling. In addition, the framework of the current model could be valuable for studying the electrokinetic and electrohydrodynamic behaviors of deformable droplets with complex compositions. Incorporating a finite viscosity ratio, membrane interfaces, and polyelectrolyte ions would enable the investigation of complex phenomena such as electrocoalescence and droplet breakup. Furthermore, the influence of impurities on the interfacial mechanical and electrical properties must be elucidated through chemical physics, in order to understand droplet electrophoresis in practical, nonidealized environments beyond pristine laboratory settings.

Acknowledgments

This work was financially supported by the National Natural Science Foundation of China (No. 12272207, 12432013). The authors would like to thank the anonymous referees who provide useful and detailed comments on the manuscript.

Conflicts of Interest

The authors declare no conflicts of interest.

Data Availability Statement

The data that support the findings of this study are available in the supporting materials of this article.

References

1. R. J. Hunter, R. H. Ottewill, and R. L. Rowell, *Zeta Potential in Colloid Science: Principles and Applications* (Academic Press, 1981).

2. J. Lyklema, *Fundamentals of Interface and Colloid Science III: Liquid-Liquid Interfaces* (Academic Press, 2000).

3. R. J. Hunter, "Recent Developments in the Electroacoustic Characterisation of Colloidal Suspensions and Emulsions," *Colloids and Surfaces A: Physicochemical and Engineering Aspects* 141, no. 1 (1998): 37–66.

4. K. G. Marinova, R. G. Alargova, N. D. Denkov, et al., "Charging of Oil-Water Interfaces due to Spontaneous Adsorption of Hydroxyl Ions," *Langmuir* 12 (1996): 2045–2051.

5. J. Baygents and D. Saville, "The Migration of Charged Drops and Bubbles in Electrolyte Gradients: Diffusiophoresis," *Physico-Chemical Hydrodynamics* 10 (1988): 543–560.

6. J. C. Baygents and D. Saville, "Electrophoresis of Drops and Bubbles," *Journal of the Chemical Society, Faraday Transactions* 87, no. 12 (1991): 1883–1898.

7. Y. Huang and M. Wang, "Electrokinetics at Liquid-Liquid Interfaces: Physical Models and Transport Mechanisms," *Advances in Colloid and Interface Science* 342 (2025): 103518.

8. V. Levich, *Physicochemical Hydrodynamics* (Fizmatgiz Moscow, 1959).

9. O. Schnitzer, I. Frankel, and E. Yariv, "Electrokinetic Flows About Conducting Drops," *Journal of Fluid Mechanics* 722 (2013): 394–423.

10. O. Schnitzer, I. Frankel, and E. Yariv, "Electrophoresis of Bubbles," *Journal of Fluid Mechanics* 753 (2014): 49–79.

11. J. Lou and E. Lee, "Diffusiophoresis of Concentrated Suspensions of Liquid Drops," *Journal of Physical Chemistry C* 112, no. 32 (2008): 12455–12462.

12. Y. Wu, L. Fan, E. Jian, and E. Lee, "Electrophoresis of a Highly Charged Dielectric Fluid Droplet in Electrolyte Solutions," *Journal of Colloid and Interface Science* 598 (2021): 358–368.

13. R. F. Probstein, *Physicochemical Hydrodynamics* (Wiley, 1994).

14. S. B. Jacob and H. Masliyah, *Electrokinetic and Colloid Transport Phenomena* (Wiley, 2006).

15. Y. Huang and M. Wang, "Electrokinetic multiphase hydrodynamics," *Applied Physics Reviews* 12, no. 3 (2025): 031322.

16. L. Onsager and R. M. Fuoss, "Irreversible Processes in Electrolytes, Diffusion, Conductance and Viscous Flow in Arbitrary Mixtures of Strong Electrolytes," *Journal of Physical Chemistry* 36 (1931): 2689–2778.

17. D. Henry, "The Cataphoresis of Suspended Particles. Part I.—The Equation of Cataphoresis," *Proceedings of the Royal Society of London: Series A* 133, no. 821 (1931): 106–129.

18. J. T. G. Overbeek, "Quantitative Interpretation of the Electrophoretic Velocity of Colloids," *Advances in Colloid Science* 3 (1950): 797–823.

19. F. Booth and N. F. Mott, "The Cataphoresis of Spherical, Solid Non-Conducting Particles in a Symmetrical Electrolyte," *Proceedings of the Royal Society of London: Series A Mathematical and Physical Sciences* 203, no. 1075 (1950): 514–533.

20. F. Booth, "The Cataphoresis of Spherical Fluid Droplets in Electrolytes," *Journal of Chemical Physics* 19, no. 11 (1951): 1331–1336.

21. R. O'Brien, "The Solution of the Electrokinetic Equations for Colloidal Particles With Thin Double Layers," *Journal of Colloid and Interface Science* 92, no. 1 (1983): 204–216.

22. H. Ohshima, T. W. Healy, and L. R. White, "Approximate Analytic Expressions for the Electrophoretic Mobility of Spherical Colloidal Particles and the Conductivity of Their Dilute Suspensions," *Journal of the Chemical Society, Faraday Transactions 2: Molecular and Chemical Physics* 79, no. 11 (1983): 1613–1628.

23. R. W. O'Brien and L. R. White, "Electrophoretic Mobility of a Spherical Colloidal Particle," *Journal of the Chemical Society, Faraday Transactions 2: Molecular and Chemical Physics* 74 (1978): 1607–1626.

24. A. J. Pascall and T. M. Squires, "Electrokinetics at Liquid/Liquid Interfaces," *Journal of Fluid Mechanics* 684 (2011): 163–191.

25. Y. Huang and M. Wang, "Solvent Mixing and Ion Partitioning Effects in Spontaneous Charging and Electrokinetic Flow of Immiscible Liquid-Liquid Interface," *Physical Review Fluids* 9, no. 10 (2024): 103701.

26. M. V. Smoluchowski, "Contribution to the Theory of Electro-Osmosis and Related Phenomena," *Bulletin International de l'Académie des Sciences de Cracovie* 3 (1903): 184–199.

27. A. Frumkin, "New Electrocapillary Phenomena," *Journal of Colloid Science* 1, no. 3 (1946): 277–291.

28. S. S. Dukhin, "Non-Equilibrium Electric Surface Phenomena," *Advances in Colloid and Interface Science* 44 (1993): 1–134.

29. E. Yariv, "An Asymptotic Deviation of the Thin-Debye-Layer Limit for Electrokinetic Phenomena," *Chemical Engineering Communications* 197, no. 1 (2009): 3–17.

30. O. Schnitzer and E. Yariv, "The Taylor-Melcher Leaky Dielectric Model as a Macroscale Electrokinetic Description," *Journal of Fluid Mechanics* 773 (2015): 1–33.

31. Y. Mori and Y. N. Young, "From Electrodiffusion Theory to the Electrohydrodynamics of Leaky Dielectrics Through the Weak Electrolyte Limit," *Journal of Fluid Mechanics* 855 (2018): 67–130.

32. P. Mahapatra and R. J. Hill, "Fluid-Sphere Electrophoresis at Low Surface Charge," *Surfaces and Interfaces* 77 (Nov. 2025): 108000, https://www.sciencedirect.com/science/article/pii/S2468023025022515.

33. S. Majhi, S. Bhattacharyya, and T. Baier, "Electrophoresis of Droplets Laden With Insoluble Ionic Surfactants Incorporating Correlations Among Finite-Sized Ions," *Journal of Fluid Mechanics* 1023 (2025): A9, edition: 2025/11/14, https://www.cambridge.org/core/product/7F5992E1AE2A3B29550CCA50695D706B.

34. R. J. Hill, "Roles of Interfacial-Exchange Kinetics and Interfacial-Charge Mobility on Fluid-Sphere Electrophoresis," *Journal of Fluid Mechanics* 1005 (2025): A1.

35. H. Ohshima, "Electrophoresis of a Weakly Charged Oil Drop in an Electrolyte Solution: Ion Adsorption and Marangoni Effects," *Colloid and Polymer Science* 303, no. 10 (Oct. 2025): 1865–1875, https://doi.org/10.1007/s00396-025-05454-z.

36. J. Lyklema, *Fundamentals of Interface and Colloid Science II: Solid-Liquid Interfaces* (Academic Press, 1995).

37. D. Jordan and A. J. Taylor, "The Electrophoretic Mobilities of Hydrocarbon Droplets in Water and Dilute Solutions of Ethyl Alcohol," *Transactions of the Faraday Society* 48 (1952): 346–355.

38. P. Mahapatra, H. Ohshima, and P. P. Gopmandal, "Electrophoresis of Dielectric and Hydrophobic Spherical Fluid Droplets Possessing Uniform Surface Charge Density," *Langmuir* 38, no. 37 (2022): 11421–11431.

39. J. Stachurski and M. MichaŁek, "The Zeta Potential of Emulsion Droplets of the Aliphatic Hydrocarbons in Aqueous Solutions," *Colloids and Surfaces* 15 (1985): 255–259.

40. P. Creux, J. Lachaise, A. Graciaa, J. K. Beattie, and A. M. Djerdjev, "Strong Specific Hydroxide Ion Binding at the Pristine Oil/Water and Air/Water Interfaces," *Journal of Physical Chemistry B* 113, no. 43 (2009): 14146–14150.

41. J. C. Baygents and D. A. Saville, "The Circulation Produced in a Drop by an Electric Field: A High Field Strength Electrokinetic Model," *AIP Conference Proceedings* 197, no. 1 (1990): 7–17.

42. M. Ma, M. R. Booty, and M. Siegel, "A Model for the Electric Field-Driven Flow and Deformation of a Drop or Vesicle in Strong Electrolyte Solutions," *Journal of Fluid Mechanics* 943 (2022): A47.

43. O. Schnitzer and E. Yariv, "Nonlinear Electrokinetic Flow About a Polarized Conducting Drop," *Physical Review E* 87, no. 4 (2013): 041002.

44. M. Z. Bazant, "Electrokinetics Meets Electrohydrodynamics," *Journal of Fluid Mechanics* 782 (2015): 1–4.

45. D. A. Saville, "Electrohydrodynamics: The Taylor-Melcher Leaky Dielectric Model," *Annual Review of Fluid Mechanics* 29, no. 1 (1997): 27–64.

46. M. van Dyke, *Perturbation Methods in Fluid Mechanics* (Parabolic Press, 1975).

47. F. Yang, S. Shin, and H. A. Stone, "Diffusiophoresis of a Charged Drop," *Journal of Fluid Mechanics* 852 (2018): 37–59.

48. O. Schnitzer and E. Yariv, "Dielectric-Solid Polarization at Strong Fields: Breakdown of Smoluchowski's Electrophoresis Formula," *Physics of Fluids* 24, no. 8 (2012): 082005.

49. L. G. Leal, *Advanced Transport Phenomena: Fluid Mechanics and Convective Transport Processes* (Cambridge University Press, 2007).

50. V. S. Markin and A. G. Volkov, "The Gibbs Free Energy of Ion Transfer Between Two Immiscible Liquids," *Electrochimica Acta* 34, no. 2 (1989): 93–107.

51. E. Megnassan, D. Le Goff, and A. Proutiere, "Dielectric Constant and Density Variations in Pure Liquids. Theoretical Relations, Comparison With Experiment," *Journal of Molecular Liquids* 59, no. 1 (1994): 37–58.

52. T. Klein, S. Yan, J. Cui, et al., "Liquid Viscosity and Surface Tension of n-Hexane, n-Octane, n-Decane, and n-Hexadecane up to 573 k by Surface Light Scattering," *Journal of Chemical & Engineering Data* 64, no. 9 (2019): 4116–4131.

53. R. Vacha, S. W. Rick, P. Jungwirth, et al., "The Orientation and Charge of Water at the Hydrophobic Oil Droplet-Water Interface," *Journal of the American Chemical Society* 133, no. 26 (2011): 10204–10210.

54. Y. Uematsu, "Electrification of Water Interface," *Journal of Physics: Condensed Matter* 33, no. 42 (2021): 423001.

55. P. Zhang, C. Chen, M. Feng, C. Sun, and X. Xu, "Hydroxide and Hydronium Ions Modulate the Dynamic Evolution of Nitrogen Nanobubbles in Water," *Journal of the American Chemical Society* 146, no. 28 (2024): 19537–19546.

56. J. Stachurski and M. Michalek, "The Effect of the Zeta Potential on the Stability of a Non-Polar Oil-in-Water Emulsion," *Journal of Colloid and Interface Science* 184, no. 2 (1996): 433–436.

57. S. Usui and T. W. Healy, "Zeta Potential of Insoluble Monolayer of Long-Chain Alcohol at the Air-Aqueous Solution Interface," *Journal of Colloid and Interface Science* 240, no. 1 (2001): 127–132.

58. J. Lützenkirchen, T. Preočanin, and N. Kallay, "A Macroscopic Water Structure Based Model for Describing Charging Phenomena at Inert Hydrophobic Surfaces in Aqueous Electrolyte Solutions," *Physical Chemistry Chemical Physics* 10, no. 32 (2008): 4946–4955.

59. D. L. Parkhurst and C. A. J. Appelo, *Description of Input and Examples for PHREEQE version 3: A Computer Program for Speciation, Batch-Reaction, One-Dimensional Transport, and Inverse Geochemical Calculations*, Report 6-A43, 2013.

60. M. Bonto, A. A. Eftekhari, and H. M. Nick, "An Overview of the Oil-Brine Interfacial Behavior and a New Surface Complexation Model," *Scientific Reports* 9, no. 1 (2019): 6072.

61. J. N. Israelachvili, *Intermolecular and Surface Forces*, Third Edition (Academic Press, 2011).

62. F. Liu and M. Wang, "Electrokinetic Mechanisms and Synergistic Effect on Ion-Tuned Wettability in Oil-Brine-Rock Systems," *Transport in Porous Media* 140, no. 1 (2021): 7–26.

63. M. Wang and A. Revil, "Electrochemical Charge of Silica Surfaces at High Ionic Strength in Narrow Channels," *Journal of Colloid and Interface Science* 343, no. 1 (2010): 381–386.

64. A. Crespy, A. Boléve, and A. Revil, "Influence of the Dukhin and Reynolds Numbers on the Apparent Zeta Potential of Granular Porous Media," *Journal of Colloid and Interface Science* 305, no. 1 (2007): 188–194.

Appendix A: Derivations of Equations (82), (84), (85), and (89)

A.1 | Derivation of Equation (82)

To do the integral of Equation (82), we first rewrite it into

$$\frac{\partial^2 V_1}{\partial Z^2} = \frac{\partial P_{-1}}{\partial \theta} - \frac{\partial^2 \Phi_1}{\partial Z^2}\frac{\partial \varphi_0}{\partial \theta} - 2\left(\frac{\partial V_0}{\partial Z} + \frac{\partial \Psi}{\partial Z}\frac{\partial \varphi_0}{\partial \theta}\right) - \frac{\partial \Psi^2}{\partial Z^2}\left(\frac{\partial \Phi_1}{\partial \theta} - Z\frac{\partial \varphi_0}{\partial \theta}\right). \tag{A1}$$

Here, the tangential pressure gradient is

$$\frac{\partial P_{-1}}{\partial \theta} = 2\frac{\partial \Psi}{\partial Z}\frac{\partial \Psi}{\partial \theta} + \frac{\partial \Psi}{\partial Z}\frac{\partial^2 \Phi_1}{\partial Z \partial \theta} + \frac{\partial \Phi_1}{\partial Z}\frac{\partial^2 \Psi}{\partial Z \partial \theta}. \tag{A2}$$

Taking advantage of the explicit expression of Ψ, it is easy to find

$$\frac{\partial \Psi}{\partial Z}\frac{\partial \Psi}{\partial \theta} = \left(-2\sinh\frac{\Psi}{2}\right)\left(-\frac{2\sinh(\Psi/2)}{\sinh\zeta}\mathcal{B}\xi_\varepsilon\Theta(\theta)\right) \equiv \frac{4\sinh^2\Psi/2}{\sinh\zeta}\mathcal{B}\xi_\varepsilon\Theta(\theta). \tag{A3}$$

Then, combining Equation (72), the original equation can be simplified as

$$\frac{\partial^2 V_1}{\partial Z^2} = 2\frac{\partial \Psi}{\partial Z}\frac{\partial \Psi}{\partial \theta} + \frac{\partial \Psi}{\partial Z}\frac{\partial^2 \Phi_1}{\partial Z \partial \theta} + \frac{\partial \Phi_1}{\partial Z}\frac{\partial^2 \Psi}{\partial Z \partial \theta} - \frac{\partial^2 \Phi_1}{\partial Z^2}\frac{\partial \varphi_0}{\partial \theta} - \frac{\partial \Psi^2}{\partial Z^2}\left(\frac{\partial \Phi_1}{\partial \theta} - Z\frac{\partial \varphi_0}{\partial \theta}\right). \tag{A4}$$

By integrating the above equation term by term from 0 to ∞, the result presented in the main text is obtained after simplification. In specific, the left-hand side gives

$$\int_0^\infty \frac{\partial^2 V_1}{\partial Z^2} dZ = \frac{\partial v_0}{\partial r} - \left.\frac{\partial V_1}{\partial Z}\right|_{Z=0}. \tag{A5}$$

The first term on the right-hand side yields

$$\int_0^\infty 2\frac{\partial \Psi}{\partial Z}\frac{\partial \Psi}{\partial \theta} dZ = \int_0^\infty \frac{8\sinh^2\Psi/2}{\sinh\zeta}\mathcal{B}\xi_\varepsilon\Theta(\theta) dZ = 4\mathcal{B}\xi_\varepsilon\Theta(\theta)\frac{\tanh(\zeta/4)}{\cosh(\zeta/2)}. \tag{A6}$$

The third term on the right-hand side yields

$$\int_0^\infty \frac{\partial \Phi_1}{\partial Z}\frac{\partial^2 \Psi}{\partial Z \partial \theta} dZ = \mathcal{B}\xi_\varepsilon\Theta(\theta)\int_0^\infty \frac{\partial \Phi_1}{\partial Z}\frac{\sinh\Psi}{\sinh\zeta} dZ, \tag{A7}$$

the integral, which can be further transformed into

$$\left(\frac{\partial \Phi_1}{\partial Z}\int_0^Z \frac{\sinh\Psi(Z')}{\sinh\zeta} dZ'\right)\Bigg|_0^\infty - \int_0^\infty \frac{\partial^2 \Phi_1}{\partial Z^2}\int_0^Z \frac{\sinh\Psi(Z')}{\sinh\zeta} dZ' dZ. \tag{A8}$$

Since $\partial\Phi_1/\partial Z$ takes the value of zero at $Z = 0$ and $Z \to \infty$, noting that $\Psi(Z') \sim \zeta e^{-Z'}$ is the fast decay function of Z', the evaluation of the above integral is about zero. Similarly the integral of the fourth term on the right-hand side is zero. The fifth term on the right-hand side gives

$$\begin{aligned}\int_0^\infty \frac{\partial \Psi^2}{\partial Z^2}\left(\frac{\partial \Phi_1}{\partial \theta} - Z\frac{\partial \varphi_0}{\partial \theta}\right) dZ &= \left[\frac{\partial \Psi}{\partial Z}\left(\frac{\partial \Phi_1}{\partial \theta} - Z\frac{\partial \varphi_0}{\partial \theta}\right)\right]\Bigg|_0^\infty - \int_0^\infty \frac{\partial \Psi}{\partial Z}\left(\frac{\partial^2 \Phi_1}{\partial Z \partial \theta} - \frac{\partial \varphi_0}{\partial \theta}\right) dZ \\ &= \left.\frac{\partial \Psi}{\partial Z}\right|_{Z=0}\frac{\partial \Phi_1}{\partial \theta} - \int_0^\infty \frac{\partial \Psi}{\partial Z}\frac{\partial^2 \Phi_1}{\partial Z \partial \theta} dZ - \zeta\frac{\partial \varphi_0}{\partial \theta}.\end{aligned} \tag{A9}$$

A.2 | Derivation of Equations (84) and (85)

Since the shear stress matching condition only depends on $\partial\Phi_1/\partial\theta$, we take the partial derivative of original governing equation on θ, giving

$$\left(\frac{\partial^2}{\partial Z^2} - \cosh\Psi\right)\frac{\partial \Phi_1}{\partial \theta} = \left(\frac{\partial c_1}{\partial \theta} - \frac{2\mathcal{B}\xi_\varepsilon\Theta(\theta)}{\sinh\zeta}\right)\sinh\Psi - \frac{\partial \varphi_1}{\partial \theta}\cosh\Psi + [c_1\cosh\Psi + (\Phi_1 - \varphi_1)\sinh\Psi]\frac{\partial \Psi}{\partial \theta}. \tag{A10}$$

To obtain the approximate solution of this equation, it is required to roughly consider the characteristics of operator $\left(\partial^2/\partial Z^2 - \cosh\Psi\right)$.

It is clearly seen that, since it contains only partial derivatives with respect to the variable Z, when applied to any function of the form $f(\theta)$, it yields $-f(\theta)\cosh\Psi$. For functions of the form $g(z)h(\Psi)$, the action of the

aforementioned operator will result in

$$\begin{aligned}
&\left(\frac{\partial^2}{\partial Z^2}-\cosh\Psi\right)\sinh\frac{\Psi}{2}=0,\\
&\left(\frac{\partial^2}{\partial Z^2}-\cosh\Psi\right)\cosh\frac{\Psi}{2}=-\cosh\frac{\Psi}{2},\\
&\left(\frac{\partial^2}{\partial Z^2}-\cosh\Psi\right)\left(Z\sinh\frac{\Psi}{2}\right)=-\sinh\Psi,\\
&\left(\frac{\partial^2}{\partial Z^2}-\cosh\Psi\right)\left(Z\cosh\frac{\Psi}{2}\right)=1-\cosh\Psi-Z\cosh\frac{\Psi}{2}.
\end{aligned}\tag{A11}$$

Then, we could write down the general form of the approximate solution to the original equation

$$\frac{\partial\Phi_1}{\partial\theta}=A_0\sinh\frac{\Psi}{2}-\left(\frac{\partial c_1}{\partial\theta}-\frac{2\mathcal{B}\xi_\varepsilon\Theta(\theta)}{\sinh\zeta}\right)Z\sinh\frac{\Psi}{2}+\frac{\partial\varphi_1}{\partial\theta},\tag{A12}$$

where we have neglected the higher-order term $\mathcal{O}(\mathcal{B})X_1$ $(X=c,\varphi,\Phi)$. Considering $\partial\Phi_1/\partial Z=0$ at $Z=0$, we have

$$\frac{\partial}{\partial Z}\left(\frac{\partial\psi}{\partial\theta}\right)=\frac{\partial^2\Psi}{\partial Z\partial\theta}=\frac{\partial}{\partial\theta}\left(\frac{\partial\psi}{\partial Z}\right)=0,\tag{A13}$$

giving the following parameters:

$$A_0=-\frac{1}{\cosh(\zeta/2)}\left(\frac{\partial c_1}{\partial\theta}-\frac{2\mathcal{B}\xi_\varepsilon\Theta(\theta)}{\sinh\zeta}\right)\tag{A14}$$

substituting which into the approximate solution will give the result (84) in the main text.

To calculate the integral in the shear stress matching condition (85), noting that the outer variable φ_1 takes the constant value (same as $r\to1_+$) within the inner region, we have

$$\frac{\partial}{\partial Z}\left(\frac{\partial\varphi_1}{\partial\theta}\right)=0,\tag{A15}$$

therefore,

$$\begin{aligned}
2\int_0^\infty\frac{\partial\Psi}{\partial Z}\frac{\partial^2\Phi_1}{\partial Z\partial\theta}dZ\equiv{}&2\left(\frac{\partial c_1}{\partial\theta}-\frac{2\mathcal{B}\xi_\varepsilon\Theta(\theta)}{\sinh\zeta}\right)\\
&\cdot\int_0^\infty\frac{\partial\Psi}{\partial Z}\frac{\partial}{\partial Z}\left[\left(Z+\frac{1}{\cosh(\zeta/2)}\right)\sinh\frac{\Psi}{2}\right]dZ.
\end{aligned}\tag{A16}$$

Setting $B_0=\cosh(\zeta/2)$, the integral in the above equation can be calculated as follows:

$$\begin{aligned}
I\equiv{}&\int_0^\infty\frac{\partial\Psi}{\partial Z}\frac{\partial}{\partial Z}\left[(Z+B_0)\sinh\frac{\Psi}{2}\right]dZ\\
={}&(Z+B_0)\sinh\frac{\Psi}{2}\frac{\partial\Psi}{\partial Z}\Big|_0^\infty-\int_0^\infty(Z+B_0)\sinh\frac{\Psi}{2}\frac{\partial^2\Psi}{\partial Z^2}dZ\\
\equiv{}&I_1+I_2,
\end{aligned}\tag{A17}$$

where

$$I_1=-2(Z+B_0)\sinh^2\frac{\Psi}{2}\Big|_0^\infty=2B_0\sinh^2\frac{\zeta}{2},\tag{A18}$$

$$\begin{aligned}
I_2=&-\int_0^\infty(-2)\left[\frac{\partial}{\partial Z}\left(\sinh\frac{\Psi}{2}\right)\right](Z+B_0)\sinh\frac{\Psi}{2}dZ\\
=&(Z+B_0)\sinh^2\frac{\Psi}{2}\Big|_0^\infty-\int_0^\infty\sinh^2\frac{\Psi}{2}dZ\\
=&-B_0\sinh^2\frac{\zeta}{2}+\frac{1}{2}\int_0^\infty\sinh\frac{\Psi}{2}\frac{\partial\Psi}{\partial Z}dZ\\
=&-B_0\sinh^2\frac{\zeta}{2}+\left(1-\cosh\frac{\zeta}{2}\right),
\end{aligned}\tag{A19}$$

$$I=I_1+I_2=\frac{\sinh^2(\zeta/2)}{\cosh(\zeta/2)}+\left(1-\cosh\frac{\zeta}{2}\right)=\frac{2\sinh^2(\zeta/4)}{\cosh(\zeta/2)}\tag{A20}$$

substituting which into the original equation will give the result (85) in the main text.

A.3 | Derivation of Equation (89)

To calculate $J_1(Z\to\infty)$, it is required to use the balance of $\mathcal{O}(1)$ terms in the advection–diffusion equation of salt concentration (24)

$$\frac{\partial J_1}{\partial Z}+\frac{1}{\sin\theta}\frac{\partial}{\partial\theta}\left(\sin\theta\cdot j_{\theta,0}\right)+\mathcal{A}U_1\frac{\partial C_0}{\partial Z}=0.\tag{A21}$$

Here, the decomposition $\boldsymbol{j}=j_r\boldsymbol{e}_r+j_\theta\boldsymbol{e}_\theta$ has been conducted, and J_1 is the $\mathcal{O}(\delta)$ term in j_r. To give the explicit form of the above equation, we need to calculate

$$j_{\theta,0}=-Q_0\frac{\partial\Phi_0}{\partial\theta}=\sinh\Psi\mathcal{B}\Theta(\theta)\left(1-\xi_\varepsilon\frac{2\sinh(\Psi/2)}{\sinh\zeta}\right),\tag{A22}$$

where we have used the results in Equation (67). Therefore, the divergence of tangential concentration flux is

$$\frac{1}{\sin\theta}\frac{\partial}{\partial\theta}\left(\sin\theta\cdot j_{\theta,0}\right)=3\mathcal{B}\sinh\Psi\cos\theta\left(1-\xi_\varepsilon\frac{2\sinh(\Psi/2)}{\sinh\zeta}\right)+\mathcal{O}(\mathcal{B}\xi_\varepsilon^2).\tag{A23}$$

Integrating from 0 to ∞ and utilizing the interface condition $J_1(Z=0)=0$, we obtain

$$\begin{aligned}
J_1(Z\to\infty)=&-3\mathcal{B}\cos\theta\int_0^\infty\sinh\Psi\left(1-\xi_\varepsilon\frac{2\sinh(\Psi/2)}{\sinh\zeta}\right)dZ\\
&-\mathcal{A}\int_0^\infty U_1\frac{\partial C_0}{\partial Z}dZ.
\end{aligned}\tag{A24}$$

Here, the contribution from higher-order terms $\mathcal{O}(\mathcal{B}\xi_\varepsilon^2)$ has been neglected.

To calculate the second term on the right-hand side term, we rewrite dC_0 as $d(C_0-1)$ and do the integration by parts, yielding

$$\int_0^\infty U_1\frac{\partial C_0}{\partial Z}dZ=U_1(C_0-1)|_0^\infty-\int_0^\infty(C_0-1)\frac{\partial U_1}{\partial Z}dZ.\tag{A25}$$

Here, the first term on the right-hand side is zero since $U_1(Z=0)=0$ and $C_0(Z\to\infty)=1$. From the $\mathcal{O}(1)$ terms in continuity equation (21), it is easy to find

$$\frac{\partial U_1}{\partial Z}=-\frac{1}{\sin\theta}\frac{\partial}{\partial\theta}(V_0\sin\theta).\tag{A26}$$

Then, the second term on the right-hand side can be further calculated as

$$\begin{aligned}
&-\int_0^\infty(C_0-1)\left[-\frac{1}{\sin\theta}\frac{\partial}{\partial\theta}(V_0\sin\theta)\right]dZ\\
=&\frac{1}{\sin\theta}\int_0^\infty(\cosh\Psi-1)\frac{\partial}{\partial\theta}(V_0\sin\theta)dZ\\
=&\frac{1}{\sin\theta}\frac{d}{d\theta}(v_0\sin\theta)\int_0^\infty(\cosh\Psi-1)dZ\\
&-3\mathcal{B}\cos\theta\int_0^\infty(\cosh\Psi-1)\left[\Psi-\xi_\varepsilon\frac{4\sinh^2(\Psi/4)}{\sinh\zeta}\right]dZ\\
&+\mathcal{O}(\mathcal{B}^2),
\end{aligned}\tag{A27}$$

where we have used the velocity matching condition (74).

To obtain the final form of $J_1(Z\to\infty)$, it is also required to calculate the following integrals:

$$\int_0^\infty\sinh\Psi dZ=2\sinh\frac{\zeta}{2},\tag{A28}$$

$$\int_0^\infty \sinh\Psi \sinh\frac{\Psi}{2} dZ = \sinh^2\frac{\zeta}{2}, \tag{A29}$$

$$\int_0^\infty (\cosh\Psi - 1) dZ = 4\sinh^2\frac{\zeta}{4}, \tag{A30}$$

$$\int_0^\infty \Psi(\cosh\Psi - 1) dZ = 2\left(\zeta\cosh\frac{\zeta}{2} - 2\sinh\frac{\zeta}{2}\right), \tag{A31}$$

$$\int_0^\infty (\cosh\Psi - 1)\sinh^2\frac{\Psi}{4} dZ = \frac{1}{4}\cosh\zeta - \cosh\frac{\zeta}{2} + \frac{3}{4} \tag{A32}$$

substituting which into the original equation will give the result (89) in the main text, where the contribution from higher-order terms $\mathcal{O}(B^2)$ has been neglected.

Appendix B: Verification of Numerical Solver for ETL Model

Here, the silica-brine surface is selected to conduct the verification of the solving algorithm for the triple-layer model and to compare it with experimental data [62]. The focus is on validating the method for solving the ζ potential and the effective surface charge density $\sigma_s = -\sigma_d$ of the independent double layer under given solution chemical environment parameters (pH, ion concentration c_i^∞).

For this charged surface system, the chemical reactions involving H^- ions at the 0-plane are

$$>\mathrm{SiOH_2^+} \leftrightarrow >\mathrm{SiOH} + \mathrm{H^+}, \tag{B1}$$

$$>\mathrm{SiOH} \leftrightarrow >\mathrm{SiO^-} + \mathrm{H^+}, \tag{B2}$$

and the chemical reaction involving M^+ ions at the β-plane is

$$>\mathrm{SiO^-} + \mathrm{M^+} \leftrightarrow >\mathrm{SiOM}, \tag{B3}$$

with the corresponding surface reaction equilibrium constants set as $\lg K_1 = 11.71$, $\lg K_2 = -6.73$, and $\lg K_\mathrm{M} = -0.25$, respectively. The total number of silanol groups at the interface remains constant, giving

$$\Gamma_0 = \Gamma_{\mathrm{SiOH}} + \Gamma_{\mathrm{SiO^-}} + \Gamma_{\mathrm{SiOH_2^+}} + \Gamma_{\mathrm{SiOM}}, \tag{B4}$$

where $\Gamma_0 = 5\ \mathrm{nm^{-2}}$. The charge densities at the 0-plane and β-plane, along with the surface densities of the surface groups ($\mathrm{nm^{-2}}$), yield

$$\sigma_0 = e(\Gamma_{\mathrm{SiOH_2^+}} - \Gamma_{\mathrm{SiO^-}} - \Gamma_{\mathrm{SiOM}}), \tag{B5}$$

$$\sigma_\beta = e\Gamma_{\mathrm{SiOM}}. \tag{B6}$$

The remaining equations are general electrostatic equations in form of planar capacitors, with the relevant capacitance parameters being $C_1 = 1.07\ \mathrm{F/m^2}$ and $C_2 = 0.2\ \mathrm{F/m^2}$.

To provide the solution for the aforementioned system, the potentials of each layer φ_i $(i = 0, \beta, d)$ and the surface densities of each surface group Γ_i $(i = +, H, -, M)$ are selected as the variables to be solved. The equations are first nondimensionalized and then solved using Newton's method. Specifically, the potentials of each layer are nondimensionalized using the thermal potential $k_\mathrm{B}T/e$ to Φ_i, the surface densities of the surface groups are nondimensionalized using Γ_0 to $\hat{\Gamma}_i$, the surface capacitances C_i $(i = 1, 2)$ are nondimensionalized using $e\sqrt{8\varepsilon_\mathrm{w}k_\mathrm{B}Tn_\infty}/k_\mathrm{B}T$ to $\hat{C}_i$, and the reaction equilibrium constants K_i $(i = 1, 2, \mathrm{M})$ are nondimensionalized using $c_{H^+}^\infty$, $c_{H^+}^\infty$, and $1/c_{M^+}^\infty$ to $\hat{K}_i$, respectively. Thus, the nondimensionalized system of equations can be written as

$$\begin{cases} f_1 = \Phi_0 - \Phi_\beta - \left(\hat{\Gamma}_+ - \hat{\Gamma}_- - \hat{\Gamma}_\mathrm{M}\right)\dfrac{\hat{\Gamma}_0}{\hat{C}_1} = 0, \\ f_2 = \Phi_\beta - \Phi_d - \sinh\left(\dfrac{\Phi_d}{2}\right)\dfrac{1}{\hat{C}_2} = 0, \\ f_3 = \left(\hat{\Gamma}_+ - \hat{\Gamma}_-\right)\hat{\Gamma}_0 - \sinh\left(\dfrac{\Phi_d}{2}\right) = 0, \\ f_4 = \hat{\Gamma}_\mathrm{H}/\hat{K}_1 - \hat{\Gamma}_+ e^{\Phi_0} = 0, \\ f_5 = \hat{\Gamma}_-/\hat{K}_2 - \hat{\Gamma}_\mathrm{H} e^{\Phi_0} = 0, \\ f_6 = \hat{\Gamma}_\mathrm{M}/\hat{K}_\mathrm{M} - \hat{\Gamma}_- e^{-\Phi_\beta} = 0, \\ f_7 = \hat{\Gamma}_\mathrm{H} + \hat{\Gamma}_- + \hat{\Gamma}_+ + \hat{\Gamma}_\mathrm{M} - 1 = 0. \end{cases} \tag{B7}$$

Denoting $\boldsymbol{x} = \left(\Phi_0, \Phi_\beta, \Phi_d, \hat{\Gamma}_+, \hat{\Gamma}_\mathrm{H}, \hat{\Gamma}_-, \hat{\Gamma}_\mathrm{M}\right)^T$, the equation set above can be written into a compact form

$$\boldsymbol{f}(\boldsymbol{x}) = 0. \tag{B8}$$

Selecting a proper initial value $\boldsymbol{x}_0$ for $\boldsymbol{x}$, the multivariable nonlinear equations can be solved using the Newton's method

$$\boldsymbol{x}_{n+1} = \boldsymbol{x}_n - \boldsymbol{J}_n^{-1} \cdot \boldsymbol{f}(\boldsymbol{x}_n) \Rightarrow \lim_{n\to\infty} \boldsymbol{f}(\boldsymbol{x}_n) = 0. \tag{B9}$$

Here, the specific form of Jacobian matrix is written as

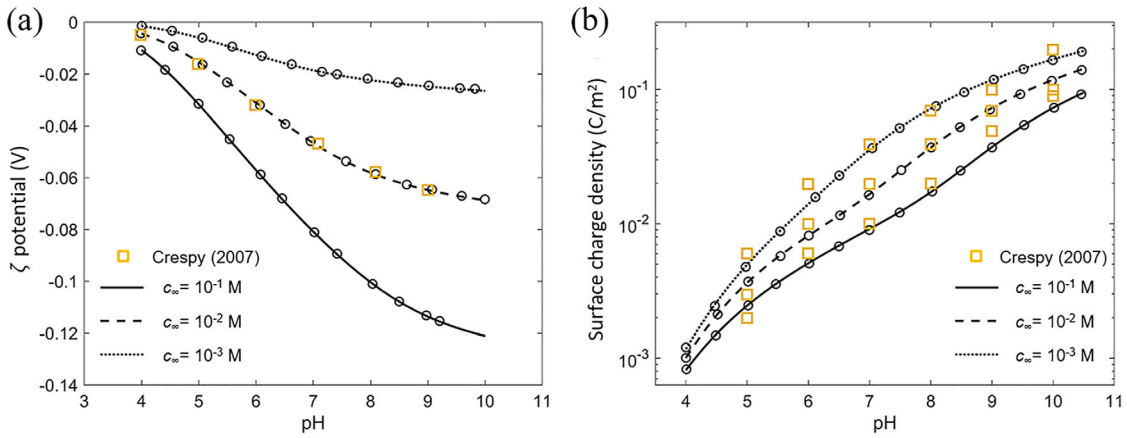

FIGURE B1 | Algorithm validation and experimental comparison of the silica-brine surface charging mechanism model, corresponding to (a) the interfacial ζ potential and (b) the interfacial charge density σ_s as functions of pH. The line graphs represent the results obtained from the charging mechanism model of this study, the circular symbols denote the results from previous models [63], and the orange square symbols indicate experimental values [64].

$$\boldsymbol{J} \equiv \frac{\partial \boldsymbol{f}}{\partial \boldsymbol{x}} = \begin{pmatrix} 1 & -1 & 0 & -\hat{\Gamma}_0/\hat{C}_1 & 0 & \hat{\Gamma}_0/\hat{C}_1 & \hat{\Gamma}_0/\hat{C}_1 \\ 0 & 1 & -1-\frac{1}{2\hat{C}_2}\cosh\frac{\Phi_d}{2} & 0 & 0 & 0 & 0 \\ 0 & 0 & -\frac{1}{2}\cosh\frac{\Phi_d}{2} & \hat{\Gamma}_0 & 0 & -\hat{\Gamma}_0 & 0 \\ -\hat{\Gamma}_+ e^{\Phi_0} & 0 & 0 & -e^{\Phi_0} & 1/\hat{K}_1 & 0 & 0 \\ -\hat{\Gamma}_{\mathrm{H}} e^{\Phi_0} & 0 & 0 & 0 & -e^{\Phi_0} & 1/\hat{K}_2 & 0 \\ 0 & \hat{\Gamma}_- e^{-\Phi_\beta} & 0 & 0 & 0 & -e^{-\Phi_\beta} & 1/\hat{K}_{\mathrm{M}} \\ 0 & 0 & 0 & 1 & 1 & 1 & 1 \end{pmatrix}. \tag{B10}$$

The corresponding calculation results are shown in Figure B1, demonstrating good agreement with the theoretical solutions of previous models and experimental values, thereby verifying the correctness of the solving procedure.